

Review

Dielectric Elastomer-Based Actuators: A Modeling and Control Review for Non-Experts

Hector Medina *, Carson Farmer and Isaac Liu

School of Engineering, Liberty University, Lynchburg, VA 24515, USA

* Correspondence: hmedina@liberty.edu

Abstract: Soft robotics are attractive to researchers and developers due to their potential for biomimicry applications across a myriad of fields, including biomedicine (e.g., surgery), the film industry (e.g., animatronics), ecology (e.g., physical ‘animats’), human–robot interactions (e.g., social robots), and others. In contrast to their rigid counterparts, soft robotics offer obvious actuation benefits, including their many degrees of freedom in motion and their potential to mimic living organisms. Many material systems have been proposed and used for soft robotic applications, involving soft actuators, sensors, and generators. This review focuses on dielectric elastomer (DE)-based actuators, which are more general electro-active polymer (EAP) smart materials. EAP-based soft robots are very attractive for various reasons: (a) energy can be efficiently (and readily) stored in electrical form; (b) both power and information can be transferred rapidly via electrical phenomena; (c) computations using electronic means are readily available. Due to their potential and benefits, DE-based actuators are attractive to researchers and developers from multiple fields. This review aims to (1) provide non-experts with an “easy-to-follow” survey of the most important aspects and challenges to consider when implementing DE-based soft actuators, and (2) emphasize current solutions and challenges related to the materials, controls, and portability of DE-based soft-actuator systems. First, we start with some fundamental functions, applications, and configurations; then, we review the material models and their selection. After, we outline material limitations and challenges along with some thermo-mechano-chemical treatments to overcome some of those limitations. Finally, we outline some of the control schemes, including modern techniques, and suggest using rewritable hardware for faster and more adaptive controls.



Citation: Medina, H.; Farmer, C.; Liu, I. Dielectric Elastomer-Based Actuators: A Modeling and Control Review for Non-Experts. *Actuators* **2024**, *13*, 151. <https://doi.org/10.3390/act13040151>

Academic Editor: Ramin Sedaghati

Received: 19 March 2024

Revised: 8 April 2024

Accepted: 13 April 2024

Published: 17 April 2024



Copyright: © 2024 by the authors. Licensee MDPI, Basel, Switzerland. This article is an open access article distributed under the terms and conditions of the Creative Commons Attribution (CC BY) license (<https://creativecommons.org/licenses/by/4.0/>).

Keywords: dielectric elastomer actuators; controls; materials modeling; FPGA; machine learning

1. Introduction

Dielectric elastomer actuators (DEAs), due to their significant potential in biomimicry applications like muscle-inspired robots, have become a major focus of research and development. Typically, DEAs are made by applying compliant electrodes to the opposite sides of an elastomeric membrane. This basic building block is then utilized to manufacture various configurations based on the application at hand. Applications can vary from displacement actuators [1–6] to deformation-based re-configurable devices [7–12]. Due to the intricate complexities of polymer networks, their deformation-dependent properties, and their dependence on external conditions, predicting the behavior of DEAs can be a complex task. Various hyperelastic and electrical models have been proposed to represent and predict their behavior. Initially, some of these models were developed from a purely mechanical perspective and applied to various elastomeric (or rubber) materials [13,14]. To account for the viscoelastic nature of DE materials, some authors have incorporated components from phenomenological or constitutive models [15–17].

Coupled with the aforementioned inherited models, many authors assumed that the electrical permittivity was constant throughout the deformation history of the material. Although this assumption has found practical use, it has been recognized that deformation

influences the level of electrical polarization within the membrane. Models that account for deformation-dependent permittivity have been proposed [18,19]. In fact, the inclusion of deformation-dependent permittivity has led to the predictions of rather unexpected behaviors [20].

Furthermore, challenges can arise related to performance limitations of existing DE materials, depending on the applications.

To address this, sometimes existing DE materials are modified via *a posteriori* treatments, such as thermo-chemical, electro-magnetic, or even doping-like processes to change their properties. Such modifications can change, for example, the material's degree of cross-linking, hence affecting stiffness and maximum stretch. Furthermore, DE materials are also synthesized to tailor the properties *a priori*. One common example is the fabrication of DE-based nanocomposites with the nanoparticle size, type, or loading aimed at prescribing certain properties or performance [21,22].

Once the soft-robotic actuator need is established and the operating conditions are defined, a material is selected, modified if needed, or fabricated. Then a suitable hyperelastic-electrical model is chosen to best approximate the expected behavior, typically based on experience or from the results of some testing/calibration procedure. Construction of the actual dielectric elastomer transducer (DET) follows based on the selected configuration, such as planar, conical, or a more complex system. When it comes to controls, the challenges can be related to various factors: the complexity of motion (expected degrees of freedom), the accuracy of the model selected, autonomy, power requirements, adaptability, size, portability (tethered or untethered systems), etc. Ultimately, soft-robotic controls, particularly DEA-based systems, have proven to be challenging [23–27]. In recent years, researchers have turned their attention to data-based approaches as a solution to the aforementioned challenges.

Moreover, adaptability and portability are still two important hurdles that need to be overcome if DE-based robots are to be autonomous and untethered. A key challenge here, as with most similar portable systems, is battery life. Another challenge is related to high-voltage requirements to actuate some DEAs. Obviously, the actual low-power required by DEAs has made the miniaturization of voltage converters a reality. More modern controls that involve machine learning are being pursued. Finally, adaptable DEA-based systems would require the so-called *reconfiguration-on-the-fly* type of firmware. With the advent of technologies that combine FPGA (field programmable gate array) and machine learning (ML), the future of adaptable DE-based robots seems attainable.

Given that a diversity of fields find the use of soft robotic systems useful, some reviews on DEA-related topics have been reported in the literature. For example, Gu et al. [28] reported a review mainly focused on applications. Later, Gupta et al. [29] reported a review that provided a survey on configurations, applications, and general challenges. Youn et al. [30] provided a review that focused on four applications of DEAs: soft robot hand, locomotion robots, wearable devices, and tunable optical components. In contrast to the aforementioned, the current review aims to provide non-experts with an “easy-to-follow” survey of the various aspects and challenges to consider when implementing DE-based soft actuators, and (2) emphasizes the current solutions and challenges related to the controls and portability of DE-based soft-robotic systems.

2. Applications/Configurations of DEAs

2.1. General Application Domains and Functionalities

DEs have been used for the following three general domains of applications (Sometimes DEs can be generalized as dielectric elastomer transducers (DETs) when referring to their general applications.): DEAs (dielectric elastomer actuators), DESs (dielectric elastomer sensors), and DEGs (dielectric elastomer generators). In terms of actual basic functionalities, these DE systems have been used in general movement, vibration control, wave manipulation, feedback, energy storage, generation, etc. (see Table 1). In the sequel, we describe some of these items; however, our review will focus on DEAs.

Table 1. A classification of a selection of DEA applications for actuation, sensing, and energy generation.

Category	Classification	Application	Sources
Actuators	Shape-Changing	Origami Structures	[31]
		Inflatable Structures	[32]
		Camouflage	[33]
	Object Control	Vibration Compensation	[34]
		Involuntary Tremor	[24]
	Movement	Valve	[35]
		Deformable Motors	[2]
		Rotary Motors	[36]
		Hexapod-like movement	[4]
		Insect-like movement	[37]
		Fish-like movement	[38]
		Loudspeaker	[39]
Spiral Proboscis Pump Actuator		[40]	
Elastomeric Pump		[41]	
Muscle-Inspired	[42]		
Electromagnetic Wave Manipulation	Frequency Selective Surfaces	[43]	
	Stretchable Microfluid Channels	[44]	
	Parasitic Elements	[11]	
	Hemispherical Ring Patch Antenna	[12]	
Optical Manipulation	Expansion-type Tunable Lenses	[10]	
	Liquid Lenses	[9]	
	Metasurface Lenses	[45]	
	Tunable Diffraction Transmission Grating	[46]	
	Tunable Resonance Filter	[47]	
Sound Isolation	Duct Silencer	[48]	
	Band gap Low Frequency Noise Filter	[49]	
Sensing	Feedback	Deformation Sensing	[50]
		Tactile Display	[51]
	Combined	McKibben Muscle Sensors	[52]
	Pressure Sensing	Multi-modal pressure-displacement sensor	[53]
		Pressure Sensing	[54]
		Audio-tactile interface	[55]
		Venus Fly-trap mimicry	[56]
Gesture Recognition	Hand Gesture Detection	[57]	
Humidity Detection	Hygromorphic DEA	[58]	
Energy Generation	Environmental	Tidal Wave Generation	[59,60]
		Wind Energy Generation	[61,62]
	Human	Heel Strike Generator	[63]
Mechanical	Crankshaft Generator	[64]	

2.1.1. Application Domains

DEAs

As actuators, DE-based materials are often referred to as artificial muscles. In its most basic form, the dielectric layer material is sandwiched between two compliant electrodes, and it deforms upon the application of an electrical potential above some threshold and below some electric breakdown limit (see Figure 1). This is because as the electric force is applied, a through-thickness electric field is induced, and the internal charges in the polymer separate (called polarization). The degree to which this polarization occurs depends on the so-called electrical permittivity. This state of affairs produces compressive

stress in the thickness of the material and produces an expansion in the surface area of the membrane. DEAs are the focus of the current review.

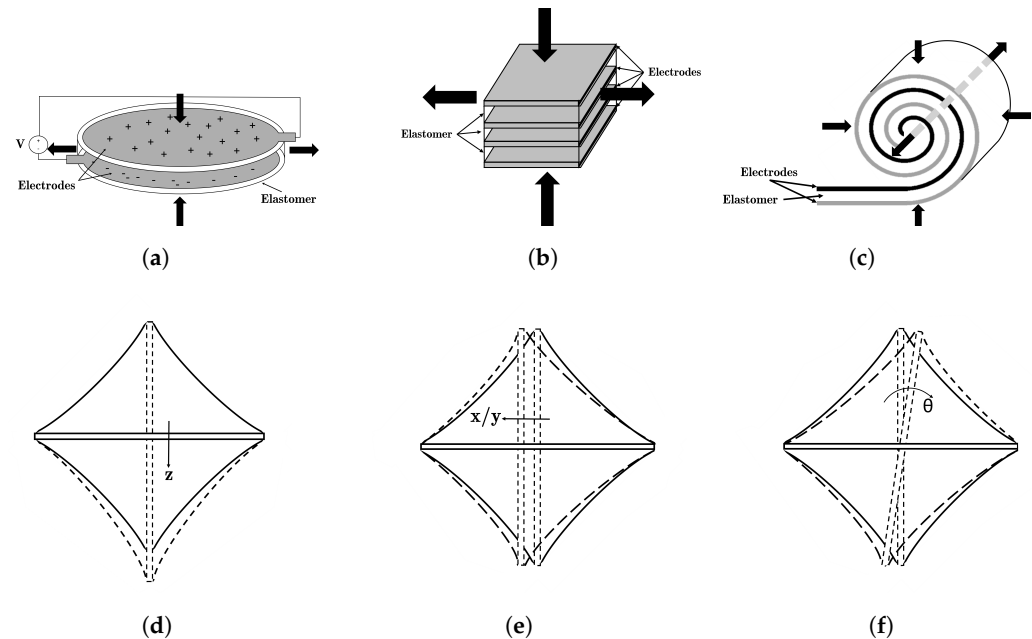


Figure 1. (a) The conventional planar DEA configuration for in-plane displacements. When a voltage, V , is applied through the thickness of the material, the resulting Maxwell stress produces an expansion in the area of the electrode region. (b) A stacked DEA configuration capable of linear displacements in the direction of the stack, and of expansion/contraction in the plane of the membranes. (c) The rolled DEA configuration is capable of linear displacements along the major axis and inversely proportional displacements in the minor axis. For the stacked DEA configuration, compression of the stack occurs during actuation while the rolled configuration expands during actuation. (d–f) More detailed motion description of double conical DEA, which has 5 degrees of freedom. The configuration exhibits a (d) vertical displacement along one axis, (e) horizontal displacements along two axes, and (f) rotation about two axes.

DESS

As sensors, DE-based systems typically rely on the change in capacitance of the material when deformations occur. The capacitance change can be determined by a suitable and sensitive electrical circuit that maps the voltage drop (due to capacitance variation) to the deformation. In contrast to DEAs, DESSs can operate at smaller voltages. DESSs will not be discussed further in this review.

DEGs

Although DEGs are not the focus of this review, it might be worth explaining them a little further since actuation can be part of their core functioning operation. DEGs could serve as a novel means to obtain energy from renewable sources or as a means to power mobile devices. Kornbluh covers several applications of DEGs [59]. The first application is a heel strike generator, which harvests energy from the wearer without adding any physical burden to the wearer. This can be used to power wearable devices. It can produce an electrical output of 0.8 J per step, or about 1 W. Each human step compresses a DEG, which produces a voltage. The second involves the use of dielectric elastomers for the harvesting of wave energy. This system uses hydrodynamic energy to stretch and contract a dielectric elastomer, which the DEG converts to energy. The example system the researchers established had an energy density of 0.1 J/g. The third is a polymer engine generator. The engine uses the expansion of gases to directly drive the expansion of a dielectric elastomer. The researchers demonstrated that a polymer cylinder can sustain the temperature of combustion and provide 11% fuel-to-mechanical efficiency. Most DEG research has focused

on the first two applications that Kornbluh presented: the harvesting of energy from fluids and the harvesting of energy from human motion. One technology to harvest energy from waves is the polymeric oscillating water column (poly-OWC). Poly-OWC is one example of a WEC DEG [65]. It is partially submerged, with the immersed part allowing waves to flow through the structure, and the upper part closed by the DEG membrane forming an air chamber. As waves flow through the structure, the induced pressure pushes the air in the unsubmerged portion, which inflates and then deflates an inflated–circular diaphragm DEG accordingly. Vertechy 2015 developed an electro-visco-elastic model for ICD-DEGs that can be easily integrated into existing OWC system models [63]. Meanwhile, research on wearable technology continued, focusing primarily on obtaining from walking motion, such as the human knee [66]. The recovery of energy from vibration has also been researched. This system works well, provided that the response is tuned to that of the vibrating structure. There is also not much evidence that DEGs can work well at high frequencies of 10 to 100 Hz [67].

2.1.2. Basic Functionalities

Movement

Movement is perhaps the most obvious application of dielectric elastomer actuators, which are often referred to as artificial muscles. Due to their unique capabilities, DEAs are useful in biomimicry applications and soft robotics [68]. Some examples include insect-inspired flapping wings [69], musculoskeletal actuation [37], and several other animal-like movements [4,38,40,69,70]. Furthermore, DEAs can mimic diaphragmatic movement, allowing fluid pumping and the creation of sound [35,41]. There are also generic applications of actuation, such as the driving of industrial valves. The primary advantage is that they are less expensive while still having similar performance [35]. DEAs can perform more than simple linear actuation tasks. They have also been used in rotary [71] and deformable motors [2].

Vibration Suppression

The strong viscoelastic properties present in some DE membranes allow for designs of vibration suppression systems by creating tunable dampeners [24,34,34,72–74]. The configuration of DEAs used in vibration suppression includes tubular [74,75], conical [34], and planar [73]. The flexibility of the DE membrane allows the shape of the DEA to influence the frequency response characteristics. Additionally, the implementation of vibration system controllers has proven effective for the geometries previously mentioned [34,73–75]. In application, DEAs are effective at mitigating the effects of pathological tremors [24,76,77].

Transformation (Structure/Property Changes)

When DEAs are combined with other structures or materials, the structures or properties change to the visible properties of the material. For example, the structure and shape of the DEA can be controlled by implementing varying stiffness components [31,78]. Aksoy and Shea used shape-memory polymers to control the location and orientation of the bending axis for a single-planar DEA [78]. By embedding heating elements into the composite membrane, the bending axis location and orientation were moved based on the heating and cooling of shape memory polymers. Similarly, the creasing of the stiff layer forms a region where bending is favorable and allows for structural changes in the DEA [31,79,80].

For this review, the second type of transformation to be considered will be a color change of the elastomer. In the case of DEA composites, the combination of DEA with stretchable photonic crystals allowed Zhao et al., to develop a color-changing DEA device responsive to deformation [81]. Furthermore, the use of monodispersed glassy silica nanoparticles in the elastomer allowed a display to be created with controllable transparency based on the degree of deformation [82]. Other studies involving the use of creating camouflaging and color-changing structures with DEAs include references [33,83,84].

Wave Manipulation

The application of DEAs in wave manipulation is interesting, as well. Tunable filtration is a specific application. By spin coating a polydimethylsiloxane (PDMS) film on a sinusoidal phase grating master and placing it on a VHB 4910 carbon black DE, Aschwanden et al., achieved a highly tunable transmission grating, with applications in communication systems, optical data storage, displays, and microscopes [46]. Wang et al. [47] built upon Aschwanden et al.'s work by creating a DEA-based guided-mode resonance filter. Such dielectric elastomer transmission gratings have a dramatic increase in tuning range compared to comparative stiff piezoelectric actuators.

Beyond filtering light, DEAs can be used in active noise filtration. For example, a circular DEA was used as a band gap filter for low-frequency noise [49]. Given that the acoustic properties of a membrane are related to tension, by simply applying various voltages to stretch the elastomer, the researchers could filter out certain frequencies and tune the filter over a range of 60 Hz. Lu et al., covered the open end of a cavity with a DEA to create an adjustable acoustic resonator. This serves as a simpler replacement for the traditional air-handling system duct silencer [48].

Reconfigurable antennas are other instances of DEA wave manipulation. The complexity and increased functionality of modern telecommunication devices make antennas with adjustable frequency, polarization, or radiation characteristics necessary to achieve optimal performance [85]. Dielectric elastomer actuator technology is of interest because it is simpler to implement than existing reconfigurable antenna technology, without requiring switching mechanisms biasing lines, or optical fiber/laser diode integration. Research focuses include monopole antennas [11], stretchable patch antennas [86,87], reconfigurable microstructure antennas [88], and adjustable patch antennas [12].

Tunable, soft lenses are other interesting wave manipulation applications of DEAs. Tunable lenses based on dielectric elastomers allow for focal length changes of more than 100% with response times of less than one second [9]. This flexibility and speed are of great use in applications ranging from robotic systems to medical imaging devices [30]. She et al., combined dielectric elastomers with metasurfaces as a thinner and lighter replacement for traditional bulk optical devices [45]. These metasurfaces contain patterns of sub-wavelength-spaced elements that shape the wavefront of transmitted, reflected, or scattered light [89]. By using DEAs to alter the size, shape, and lateral translations of the metasurface, She et al., could tune the focal length, astigmatism correction, and image shift control of the metasurface. Nam et al., specifically applied this technology to a tunable camera application [10].

2.1.3. Feedback

Another application of DEs involves using DEs for feedback. An example is the use of DEs for a portable force feedback glove [50]. The authors of this study manufactured spring roll DE actuators. These sensors can be implemented in conjunction with DEA to create self-sensing actuator technology [90] or in tactile displays [51]. For further reading on self-sensing DEA configurations, see [25,91].

2.2. Configurations

2.2.1. Planar Actuators

The development of planar dielectric elastomers, which for the purposes of this review, focuses on a single DEA membrane without an applied out-of-plane force (see Figure 1).

Chortoes et al., developed a method to manufacture DEAs with dispersed electrodes in an elastomeric matrix [92]. The new method of manufacturing DEAs resulted in the creation of actuators capable of contractile deformations. The manufacturing method required a custom 3D printing system and further research is required to develop the system.

Furthermore, Hajiesmaili et al., developed a method to manufacture thinly layered DEAs with overlapping electrodes to produce DEAs that can deform into shapes with

positive, negative, or positive and negative Gaussian curvatures [8]. By controlling the amount of overlap between opposing electrodes, the actuated curvature of the membrane could be controlled and predicted.

The design of the electrodes can be used to predict the final shape of the DEA when voltage is applied; however, an inverse mapping from the final shape to the required electrode pattern is not provided and demonstrates an open research area.

By applying a minimum energy structure approach to DEAs, the normally rigid frame is substituted with a flexible and deformable frame. The deformations of the frame and DEA can be found by finding the state of minimum energy. Zou and Gu examined using the minimum energy structure approach for modeling bending and flexible DEA structures [93]. They examined creating a minimum energy structure hinge to allow for bending deformation. Future research for the study of minimum energy structures would allow for a reverse approach of given a set of displacements and boundary conditions to find a suitable frame design.

Li et al., examined the modes of actuation present in a DEA and designed a “zipping” configuration, where a conductive plate was placed below the elastomer [94].

A voltage was applied between the plate and the surface of the elastomer furthest from the plate. The voltage differential attracted the elastomer towards the plate in a mode described as “zipping”. The zipping mode improved the overall performance of the DEA, allowing for a voltage differential greater than the breakdown voltage to be applied. Furthermore, they demonstrated that constructing a joint with the “zipping” mode allowed them to move a table tennis ball.

In regard to creating actuators capable of robotic locomotion, Christianson et al., created a submersible DEA where the internal chamber was filled with a conductive fluid connected to a voltage supply [3]. The surrounding liquid bath is another conductive fluid that is connected to the ground. By applying a voltage to the internal fluidic channel, a swimming motion can be achieved similar to that of an electric eel and mimicking the movement. With further research, a self-contained DEA swimming application can be created to allow for the autonomous operation. To create terrestrial locomotion, Minaminosono et al., developed a deformable DEA motor [2]. The motor functioned by actuating different quadrants of a DEA to rotate an eccentric shaft that would rotate. Their study investigated how deformation affects the speed of the motor. Further research on DEA-driven motors could produce useful innovation for creating soft and flexible motors for robotic applications. With the examination of locomotion focused on DEAs, Jia et al., examined the in-plane resonance of DEAs by applying a varying frequency sinusoidal voltage to a VHB4905 DEA [95]. The configuration exhibited a natural frequency of 30 Hz and a super-harmonic frequency of 500 Hz for a pre-stretch of 1.05. The results from the experimental study were able to be verified by using a Neo–Hookean material model combined with a viscous dampening component. Further development of in-plane and out-of-plane resonance could produce new applications for single-actuator vibration control and possibly locomotion. In developing locomotion based on soft actuators, a traditional motor rotates while DEAs are often used for linear movement. By designing a unique electrode pattern Waché et al., was able to design a DEA capable of producing up to 10° of rotational movement [36]. The different DEA configurations provide a glimpse into the possible methods for achieving a controlled location device based on dielectric elastomers.

2.2.2. Conical Actuators

A unique structure for the exploration of DEAs is the conical configuration which is produced by applying an out-of-plane force to the DEA membrane. When combined in an antagonistic configuration, the resulting system is capable of multiple degrees of freedom [4,96,97]. The deformation in the vertical direction of a single out-of-plane actuator has been characterized by He et al. [98]. In predicting the behavior of certain systems, the edges of the cone can be assumed to be straight for either small structures or high pre-stretches. In both cases, the curvature of the film is reduced and can be assumed to

be straight. Furthermore, resonant effects of the material can be harnessed for various movement applications as demonstrated by Cao et al. [99]. Xue et al., demonstrated that the use of a single conical elastomer system can be used to develop a modular crawling robot [100]. Previously, research was required to improve the modeling of the nonlinear material behavior and multi-domain coupling. For instance, Farmer and Medina showed that for certain electro-mechanical coupling values, instabilities are introduced into the actuation mechanism for the CDEA [20]. Similarly, combining the CDEA configuration with a bi-stable spring forms a controllable bi-stable oscillator which can lead to chaotic behavior [101].

With the various non-linearities present in the material, the prediction of the deformation of the CDEA configuration remains challenging with the only analytical approach being for vertical displacement of the CDEA [98]. Medina and Farmer then proposed an approximate model based on empirical data to predict the horizontal and vertical displacements of the double cone configuration [96]. While challenges remain in the analytical modeling of the CDEA configuration, the displacement control is possible by neural networks [102], modern control methods [103], and traditional approaches [104]. As refinements are made to both the analytical approaches to modeling the CDEA deformation along with the controller, new methods of locomotion for robotics are expected.

2.2.3. Complex Structures

While studying simple planar or conical DEAs allows for a basic understanding of the mechanics of the device, combining multiple DEAs allows for unique applications in vibration control [76], locomotion [5,105], and bio-inspired design [6,38]. Hoffstadt and Mass developed a stacked DEA which was controlled by an extended Kalman filter (EKF) [27]. The EKF was responsible for determining the resistance and capacitance of the stacked DEA material. From the EKF, the resistance and capacitance of the stack were measured from the voltage and current applied to the DEA. The EKF test setup was tested with both a laboratory-grade voltage amplifier and a bidirectional flyback converter. The results demonstrated that the control of the stacked DEA was independent of the quality of the power supply. They found that their system was accurate for small strains (<3%). Kelley et al., implemented a stacked dielectric elastomer actuator to limit the effects of involuntary tremors on daily life [76]. A system of stacked DEAs attached to the wrist of the user provided a method for limiting involuntary tremors based on the frequency. The frequencies of the voluntary and involuntary movements were analyzed and a band-limited multiple Fourier linear combiner to identify the tremor components of the patient's movements. Using data from [106], Kelley and Kauffman demonstrated that the control system was able to identify and limit involuntary tremors. When the movement is voluntary, the user is required to move against the resistance of the DEA system.

By combining rigid fibers and multi-layer DEAs, Duduta, Clarke, and Wood developed a micro-crawling device [5]. The DEAs facilitated locomotion by expanding outwardly against single-wall carbon nanotubes (SWCNTs) that were stamped onto the elastomer as it was cast. The SWCNTs provide a rigid structure in the DEA creating a bending actuation. After creating a multi-DEA system, the group achieved locomotion of approximately 1.03 body lengths per second. The method of creating a multi-layered DEA system allowed for improved actuation compared to the use of a single elastomer layer. Sun et al., connected multiple DEAs to construct a folding device capable of locomotion [105]. By connecting a rigid link to an elastic hinge, the four DEAs were connected to allow for deformation of the structure. When the DEA system was attached to a wheel structure, the device achieved a maximum velocity of approximately 40 mm/s. By wrapping a linear spring with a DEA, Zhang et al., created a spring roll actuator capable of existing in four unique states depending on the force and voltage applied to the spring roll [50]. As bio-inspired systems begin to become smaller, the ability for DEAs and other smart materials to mimic animals becomes more prevalent. One such example is a firefly-like DEA with an ethyl cellulose backing allowing the DEA to mimic the flapping motion of insect wings [31]. The

use of cellulose paper allowed for the implementation of a light-producing and locomotion-capable system. With further developments to the system, origami-inspired folding devices could be created. In creating a bio-inspired underwater device, Shintake et al., developed a fish-like DEA system capable of swimming in low Reynolds number flows with a similar Strouhal number of a fish [38]. A more extensive review of DEA applications is explored in the next section.

2.3. Design Optimization Techniques

The various nonlinear effects, such as deformation-dependent permittivity, visco-hyperelastic behavior, and dielectric relaxation, form a challenging nonlinear optimization problem for DEA designers [6,107–112]. For instance, Chen et al., proposed using level-set methods for optimizing the electrode geometry for planar DEAs for moving points on the plane [108]. Further, Wang et al., developed a method for optimizing the structure of DE minimum energy structures (DEMESs) by representing the complaint frame with fat Bezier curves. The design optimization process optimized the structures for three-dimensional shapes [6]. Furthermore, Wang et al., utilized a genetic algorithm for optimizing the electrode placement in planar DEAs [6]. They utilized a finite element grid, where each element was in either an actuated or unactuated state. Following the finite element analysis formulation of [110], they found optimal electrode patterns for linear displacement of a stiff rod in the DEA along with rotation of a stiff rod and cross. From the study, the genetic algorithm was noted to have issues with creating patterns with holes or disconnections. Lastly, Garnell et al. [111] utilized a level-set method to optimize the electrode topology for a dynamic loud-speaker application. The optimized geometries were experimentally validated to match the computational model developed. While the area of geometry optimization for DEAs shows promise for electrode and rigid support design, the areas of material optimization and three-dimensional geometries have remained largely untouched.

3. Material Models

For the prediction of DEA behavior, the stress–strain relationship in the material must be understood. Compared to metals which exhibit a highly crystalline structure, polymer networks exhibit essentially no symmetry and contain randomly oriented polymer chains, in general. The modeling process for dielectric elastomers begins with determining the key characteristics of the application such as the operating temperature, strain rate, and cross-linking density (see Figure 2). Next, the selection of a material model is required to determine the stress–strain relationship and possibly the visco-elastic response of the material. The material modeling approaches can be classified into two categories: statistical and phenomenological. First, the statistical approach analyzes the behavior of polymer chains and the probability distributions associated with the individual chain segments. Different statistical approaches have aimed to determine the deformation of the polymer chains and thereby the stress and strain of the material subjected to a load [113–116]. Then, phenomenological approaches have determined the stress–strain relationship through the use of invariants to empirically determine material behavior [13,117–121]. Following the selection of a material model, the parameters in the model are selected based on either known material properties, mechanical testing, or a combination of the two. Once the hyperelastic model is determined, the behavior of dielectric elastomers actuators is predicted by summing the electrical and the mechanical energy domains, W_E and W_M respectively, in the system:

$$W_T = W_M + W_E \quad (1)$$

where W_T is the total energy.

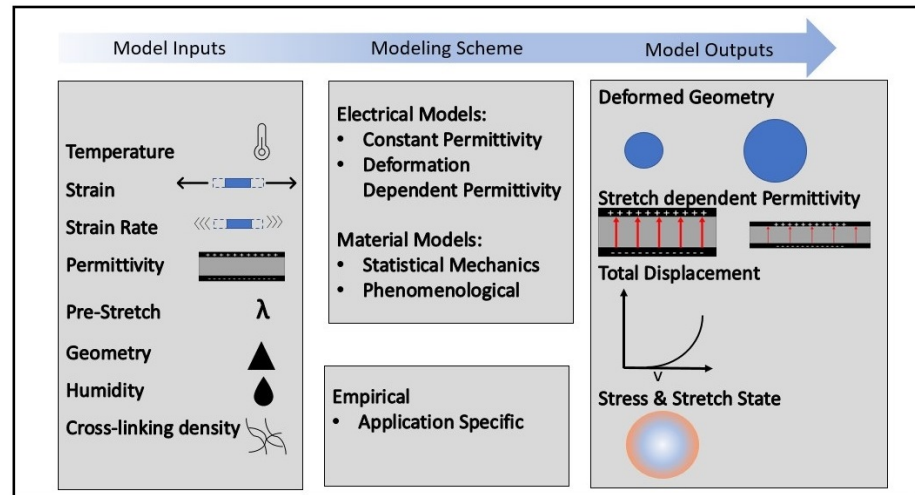


Figure 2. A graphical description of the modeling process required for predicting the behavior of dielectric elastomer actuators.

3.1. Hyperelasticity

Elastomeric behavior is mostly analyzed via fundamentals of continuum mechanics. Assuming that the material is isotropic, hyperelastic, and homogeneous, the strain energy can be expressed in terms of the three invariants:

$$I_1 = \lambda_1^2 + \lambda_2^2 + \lambda_3^2 \tag{2}$$

$$I_2 = \lambda_1^2\lambda_2^2 + \lambda_2^2\lambda_3^2 + \lambda_3^2\lambda_1^2 \tag{3}$$

$$I_3 = \lambda_1^2\lambda_2^2\lambda_3^2 \tag{4}$$

where $\lambda_1, \lambda_2,$ and λ_3 are the principal stretches. If the elastomer is assumed incompressible—a reasonable assumption for the materials being used in the manufacturing of soft actuators—then the third invariant is equal to unity. Possible hyperelastic material models used to predict the mechanical behavior of dielectric elastomers include the following:

- Mooney–Rivlin [119]

$$W_M = \sum_{i,j=0}^{\infty} C_{ij}(I_1 - 3)^i(I_2 - 3)^j \tag{5}$$

where C_{ij} denotes material constants found from best-fitting stress–strain data.

- Neo–Hookean [122]

$$W_N = \frac{\mu}{2}(I_1 - 3) \tag{6}$$

where μ is the small strain shear modulus.

- Ogden [121]

$$W_O = \sum_{p=1}^N \frac{\mu_p}{\alpha_p} (\lambda_1^{\alpha_p} + \lambda_2^{\alpha_p} + \lambda_3^{\alpha_p} - 3) \tag{7}$$

where μ_p and α_p are material constants determined from best-fitting stress–strain data.

- Gent [13]

$$W_G = -\frac{\mu J_m}{2} \log \left(1 - \frac{I_1 - 3}{J_m} \right) \tag{8}$$

where J_m represents the limiting stretch in the material.

- Yeoh [120]

$$W_Y = \sum_{p=1}^N C_p (I_1 - 3)^p \quad (9)$$

where C_p are material constants determined by best-fitting stress–strain data.

- Arruda–Boyce [113]

$$W_{AB} = Nk_b\theta\sqrt{n} \left[\beta\lambda_{chain} - \sqrt{n} \log \left(\frac{\sinh \beta}{\beta} \right) \right] \quad (10)$$

where N is the number of unit chains, k_b is the Boltzmann constant, θ is the absolute temperature, β is the inverse Langevin function of r_{chain}/Nl , where r_{chain} is the unit chain length, l is the chain length, n is the chain density, and λ_{chain} is the limiting stretch of the chain.

- General Constitutive Model [115]

$$W_{GC} = G_c N \ln \left(\frac{3N + \frac{1}{2}I_1}{3N - I_1} \right) + G_e \sum_i \frac{1}{\lambda_i} \quad (11)$$

where G_c is the initial network modulus and G_e is the entanglement modulus.

- Edwards–Vilgis [114]

$$W_{EV}(\lambda_1, \lambda_2) = \frac{1}{2} N_C^* \left[\frac{(1 - \alpha^2)I_1}{1 - \alpha^2 I_1} + \log(1 - \alpha^2 I_1) \right] + \frac{1}{2} N_S^* \left[\sum_{i=1}^3 \left\{ \frac{(1 + \eta)(1 - \alpha^2)\lambda_i^2}{9 + \eta\lambda_i^2(1 - \alpha^2 I_1)} + \log(1 + \eta\lambda_i^2) \right\} + \log(1 - \alpha^2 I_1) \right] \quad (12)$$

where $N_C^* = N_c k_b T$, $N_S^* = N_s k_b T$. N_C represents the number of cross-links per volume. N_S represents the number of sliplinks per volume. Finally, α and η represent the measurement of chain extensibility and average slip displacement, respectively.

- Nonaffine Network [116]

$$W_{NaN} = \frac{1}{6} G_c \sum_{j=1}^3 \lambda_j^2 - G_c \lambda_{max}^2 \ln \left(3\lambda_{max}^2 - \sum_{j=1}^3 \lambda_j^2 \right) + G_e \sum_{j=1}^3 \left(\lambda_j + \frac{1}{\lambda_j} \right) \quad (13)$$

where λ_{max} is the maximum stretch of the affine vector.

Recently, Farmer and Medina implemented a large number of hyperelastic material models for the modeling of soft materials [123]. This included the development of a Julia library containing the largest, to date, collection of hyperelastic material models in existence. The package provides a set of analytical and data-driven strain energy density functions (SEDFs) and the tools required to calibrate the models to material tests. The package is designed to leverage multiple dispatch in defining a common set of functions for calculating the strain energy density function (SEDF), the second Piola–Kirchhoff stress tensor, and the Cauchy stress tensor.

3.2. Deformation-Dependent Permittivity

Within the electrical domain, it is assumed that the elastomer film behaves similarly to a polymer melt [124]. The free energy of the electrical domain is determined by the following:

$$W_E = \frac{D^2}{2\varepsilon(\lambda_1, \lambda_2, \lambda_3)} \quad (14)$$

where D is the true electrical displacement and ε is the dielectric permittivity of the material. Often, the dielectric permittivity is assumed to remain constant throughout the deformation;

however, recent studies have shown that the constant permittivity assumption is not valid in the large deformation region [18,19,125].

A common assumption when modeling DEA systems is that the dielectric permittivity remains constant with deformation; however, several experimental studies have shown that the dielectric permittivity is highly dependent on the deformation state of the DE membrane [125–128]. Following the framework of Kuhn and Gruhn [129], different studies have found analytical solutions for the relationship between deformation and permittivity [18,19]. Opris et al., found that by blending a silicone elastomer with poly(divinylbenzene) (PVDB), the dielectric permittivity of the material could be increased allowing for a larger actuation at a small applied voltage. Other approaches include a temperature dependence introduced by [130], which utilizes a framework based on the Debye model for the dielectric constant of a gas and an empirical approach to fit the desired characteristics. Following the derivation set forth in [19] and assuming incompressibility, the resulting equation for the deformation-dependent dielectric permittivity, ε , is

$$\varepsilon(I_1) = \varepsilon_0 + c f(I_1/I_m)(\lambda_3 - \frac{1}{3}I_1) \quad (15)$$

where ε_0 is the undeformed permittivity, $f(I_1/I_m) = 1 + 1/3(I_1/I_m) + 1/3(I_1/I_m)^2$, which represents the sensitivity of the permittivity to deformation, c is the electrostriction coefficient and I_m is the first invariant at the limiting chain stretch. The full derivation of the equation is presented in [19].

3.3. Other Considerations for Material Modeling Include the Effect of Hysteresis

In this section, we provide some introductory guidelines to the topic of hysteresis as it relates to elastomeric materials modeling, in general. Further modeling schemes should be sought elsewhere, and the interested reader is directed to some relevant literature [131–150], as a starting point.

Mechanical hysteresis is defined as the difference between the loading and unloading behavior based on a fixed strain (or stretch) rate. However, this difference can be affected by the strain rate [138], as well as by temperature [139] and other microstructural features, such as the degree of cross-linking [140], entanglement, and nanoparticle loading (i.e., concentration) in particle-filled material-based DEs (e.g., polymer nanocomposites). The literature shows that rheological models containing elastic and slip elements are derived from a general pure hysteresis model, which is what Lion referred to as equilibrium hysteresis [141]. It could be related to the relaxed equilibrium response within cyclic deformation and is usually attributed to plastic effects by some authors [144,145]. Some other authors use the theory of viscoplasticity to reproduce a similar behavior [142,146]. However, if the equilibrium hysteresis appears to be negligible, a viscoelasticity theory is sometimes sufficient to represent it, as reported in the literature [140,143,147–149]. In the particular case of elastomers filled with particles, a physical interpretation, in terms of irreversible slip processes between adjacent filler particles, has been reported [150].

4. Material Limitations and Challenges

While processing commercially available elastomeric films or manufacturing custom-tailored films reduces some of the inherent challenges associated with controlling and modeling dielectric elastomers, multiple challenges still persist when using these materials for actuators or sensors. First, limitations occur in regions of the electromechanical operating range where the material can rapidly begin to thin in response to the applied electric field which can lead to tearing or failure of the material [151,152]. Furthermore, inhomogeneities within the material lead to potential wrinkling and instability regions at the limits of the actuation [153–156]. Next, the material will exhibit a specific dielectric breakdown limit, which sets a limit on the upper bound of actuation without electrical failure of the material [157,158]. Moreover, different dielectric elastomers can exhibit increased actuation in response to having a pre-applied load or pre-stretching the film [152,159]. The

application of pre-stretching often limits the usefulness of the dielectric elastomer because it requires some type of rigid mechanism to maintain the pre-stretch. These limitations provide physical limits to the application of dielectric elastomers for actuation and create modeling challenges for predicting the behavior when operating near these limiting values.

4.1. Electro-Mechanical Instabilities

With a variety of behaviors present in DEs, the various stretch-stress relationships need to be “tuned” for optimal performance. One way to tune the actuators is by pre-stretching the membrane. The pre-stretch first induces an initial stress in the membrane prior to electrical loading. Next, the applied stress causes a thinning of the material that increases the electric field at a given voltage. The applied stretch has been shown to increase the overall performance of acrylic dielectric elastomers [160]. Li et al., found that the effects of electro-mechanical instability can be reduced by pre-stretching the dielectric elastomer film [152]. Zhao and Suo showed that the non-monotonic relationship between voltage and stretch in a dielectric elastomer can cause the film to fail [161]. However, pre-stretching the membrane allows for improved performance by altering the shape of the voltage-strain curve. Recently, Mathew et al., showed that the phenomena of sliplinks in polymer networks can contribute to electromechanical instabilities [151]. When using the Edwards–Vilgis model [114] to fit the experimental data for VHB 4905, there were more than two sliplinks to every cross-link. By comparing the Edwards–Vilgis model to the Gent model, consideration of polymer sliplinks revealed a mode of instability that is not observed when using the Gent model.

4.2. Wrinkling

When inhomogeneities occur in the material either as a result of material processing or electrode application, the elastomer has been shown to wrinkle, buckle, or crumple under high electric fields [153–156]. Plante and Dubowsky were among the first groups to highlight the wrinkling that occurs in dielectric elastomer actuators [153]. They recognized that stable wrinkles can occur in DEAs under particular conditions. The observed wrinkles were shown to occur before the pull-in instability occurred. The pull-in instability appears when equilibrium cannot be reached between the Maxwell stress and the principal stress in the material [124]. The pull-in instability results in a rapid thinning of the material and eventually dielectric breakdown. They noted that the point of pull-in instability and wrinkling occurring is highly dependent on the stretch rate for VHB 4905/4910. Later, Zhu et al., investigated the transition modes of a planar actuator from the flat state to the wrinkled state [155]. They observed that the first mode of wrinkling occurs in small regions of the DEA and rapidly increases as the voltage is applied. The first mode depends on the viscoelastic properties, and wrinkles can continue to grow with time. The second mode occurs instantaneously throughout the entire material. The second mode does not have wrinkle nucleation sites forming compared to the first mode. They noted that the first mode generally occurs at lower pre-stretches as compared to the second mode. More recently, Godaba et al., sought to characterize the different forms of loss of tension that can occur in DEAs [154]. First, they noted that buckling occurs at small pre-stretch values. The buckling instability was characterized by a smooth out-of-plane deformation of the DEA. Next, at intermediate pre-stretches, the membrane wrinkled, which was characterized by a lack of in-plane tension. The wrinkles remain in-plane due to flat regions with portions of the membrane buckling out-of-plane. Lastly, crumpling occurred at large pre-stretches and was characterized by out-of-plane deformation with concentrated regions of stress. The crumpling is noticeably different from buckling because crumpling has a more chaotic out-of-plane deformation compared to the smooth out-of-plane deformation that occurs in buckling. To harness the loss of tension that occurs at the onset of wrinkling, Mao et al., characterized the morphology of the amplitude of the wrinkling that occurred in the DEA [156]. By pre-stretching the membrane in a single direction, the direction of wrinkling formation could be controlled. By examining the mechanics of wrinkling in a hyperelastic

material using the Kirchhoff–Love plate theory, they were able to predict the wavelength of the wrinkles that occurred in the DEA. Their methods successfully predicted the wrinkle wavelengths of VHB9473, 4910, and 4905.

4.3. Electrical Breakdown

As a result of inhomogeneous regions within the elastomer and the electrode, different regions of the film can be subjected to different electric fields. This can cause certain areas to deform more than others. By analyzing the response of the elastomer to an electric field, certain portions of the voltage–stretch curve can become non-monotonic. The changing curvature produces a sudden jump in the stretch of the dielectric elastomer, which can potentially cause the material to fail. The electromechanical instability occurs as the elastomer thins in response to the true electric field created by the applied voltage and drastically begins thinning at a certain voltage increasing the true electric field past the breakdown field which results in electromechanical breakdown. Zurlo and DeTommase [157] experimentally demonstrated the thinning to failure of the DE membrane and the resulting thinning that occurs prior to dielectric breakdown. Liu et al. [162] demonstrated that by changing the operating temperature of the DEA, the voltage at which electromechanical instabilities occur can be reduced. By studying VHB 4905, Huang et al., found that the electric breakdown strength of VHB 4910 is determined by the stretch and thickness of the materials [163]. They found that the electric breakdown field, E_b , could be characterized by the following:

$$E_b = 51h^{-0.25}\lambda^{0.63} \quad (16)$$

where h is the thickness and λ is the stretch in the material. With the use of acrylic elastomers such as VHB, the applied voltage is in the range of approximately 5–6 kilovolts for maximum actuation [164]. To create DEAs capable of low-voltage deformation, the thickness must be decreased and the dielectric permittivity increased to allow for larger actuation at lower voltages. Recently, Sheima et al., developed a DE membrane capable of actuation of $\approx 15\%$ at 300 V [158]. Similarly, Zhao et al., formulated an acrylic-based DE, which did not require pre-stretching to achieve large actuation at low voltages [165]. They report that the elastomer achieved actuation 4.2 times greater than VHB4910 at comparable electric fields.

4.4. Pre-Stretch

When using certain DEs the membrane has been shown to exhibit larger deformations when pre-stretched [166]. Early in the study of DEAs, Kofod investigated the performance improvements that result from the pre-stretching of the DE membrane [164]. Li et al., found that by increasing the pre-stretch of the DE membrane, the likelihood of pull-in instability could be eliminated by generating electrostriction, improving the breakdown strength, and decreasing the applied voltage [152]. Using VHB 4910, he reported that by increasing the pre-stretch, a larger in-plane displacement was achieved when compared to an unstretched membrane at the same voltage. If the DE is assumed to have deformation-dependent permittivity, the pre-stretch will affect the actuation in the DEAs [159]. Kumar and Sarangi developed a model for the dielectric permittivity of the material when subjected to different pre-stretches and applied frequencies. When investigating the displacement of conical DEAs (CDEAs), Khanh et al., found that increasing the pre-stretch in a CDEA with constant force increased actuation [167].

4.5. Other Limitations

Other limitations can be related to mechanical damping, creep, and environmental factors, such as temperature and humidity. Mechanical damping and creep are greater than that of natural muscle [168] and electroactive ceramics such as BaTiO₃ [169]. Early claims [35,168] suggested that creep would not significantly affect most applications, though more recent studies suggest that viscoelastic behavior can degrade motion performance [170] and cause energy loss [171]. In terms of environmental tolerance, manufacturer

specifications and preliminary testing by Kornbluh et al., suggest operating temperatures of $-50\text{ }^{\circ}\text{C}$ to $260\text{ }^{\circ}\text{C}$ for silicone materials and $-10\text{ }^{\circ}\text{C}$ to $70\text{ }^{\circ}\text{C}$ for acrylics. However, unpublished Bayer MaterialScience results cited by Biggs et al., indicate VHB 4910 (an acrylic) has 25% lower stroke/mm outside the $0\text{--}70\text{ }^{\circ}\text{C}$ range than at $25\text{ }^{\circ}\text{C}$. Although Kornbluh et al., implied that humidity had little effect, more recent studies indicate that increased humidity increases induced deformation [172–174], increases current leakage [58], and decreases the dielectric breakdown strength of VHB 4910 [175] so that it can be exploited in humidity sensor applications [58]. Similar effects on dielectric breakdown strength were reported for silicone elastomers, though not to the same extent as acrylic [175]. Due to the complex effects of pre-stretch dependence, wrinkling, and viscoelastic effects, the controllability of DEAs is significantly limited when applying traditional control techniques. Such techniques often require some combination of system linearization, restriction of the actuation domain, and/or neglecting certain effects.

5. Treatments of Dielectric Elastomers

To overcome the limitations of DE materials, various *a posteriori* strategies are implemented. For example, Figure 3 visually illustrates the three methods used to chemically increase dielectric permittivity: polar grafting, adding fillers, and blending. Besides those shown in the aforementioned figure, other treatments and objectives are discussed in the sequel.

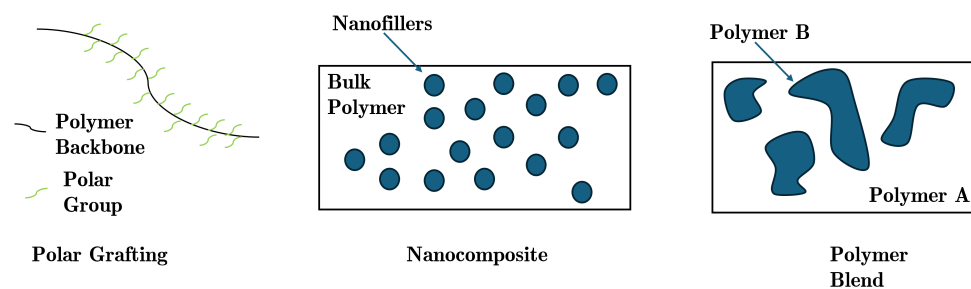


Figure 3. By using fabrication methods such as (1) polar grafting, where polar groups are attached to the polymer backbone, (2) nano-filling, where nanofillers are added to produce potentially large changes in the macroscopic properties, and (3) polymer blending, where polymers of different types are combined to produce a mixture with improved properties, the dielectric permittivity of the DE can be tuned to achieve the desired performance.

This review briefly covers strategies for the development and modification of novel DE materials. Ideal elastomer performance depends both on electrical and mechanical material properties. Using an analytical model and experimental verification of that model, Plante and Dubowsky found that DEA performance depends on pull-in failure, dielectric strength failure, viscoelasticity, and current leakage [176]. They characterized successful DEA design as dependent on balancing performance and reliability. Matthew and Koh distinguished between actuator failure and user-imposed limits, classifying material rupture and electrical breakdown as material failures and tension loss as a user-imposed limit [177]. They did not consider pull-in instabilities (referred to as electro-mechanical instabilities), as they regarded them as a precursor to either material rupture or electric breakdown. There is evidence of other instabilities, such as Rayleigh–Plateau instabilities [178] and slip-link instabilities [151]. However, current modification techniques focus on increasing performance and reliability by reducing hysteresis, increasing electrical breakdown strength, and increasing elastic toughness [179]. Pre-stretching [152,164,179], interpenetration [180–183], self-healing [184–186], blending [187,188], adding fillers [189–193], and polar grafting have been explored to achieve these goals.

Several reviews of the existing literature discuss the strategies reviewed in this paper, including Romasanta et al.’s overview of dielectric elastomers from the material perspective [179], Banet et al.’s overview of elastomer performance [194], and Skov and Yu’s review

of modification techniques for silicone-based elastomers [195]. The interested reader is directed to those reviews for further knowledge.

5.1. Interpenetration

It is well accepted in the literature that pre-stretch reduces failure by decreasing pull-in instabilities, increasing dielectric breakdown strength, and reducing viscoelasticity [152,164,179]. Supporting the pre-stretch, however, causes complications. Often, the weight of the supporting structure occupies more space than the films themselves. There is also a decrease in the lifetime of the actuator because of stress concentration between the support and elastomer. Actuator shock tolerance is also reduced, and performance can be decreased due to stress relaxation. Interpenetrating networks resolve the issue, in a sense by freezing the pre-stretch. An interpenetrating polymer network (IPN) can eliminate the need for an external pre-stretch supporting structure. Much of the post-treatment work on VHB 4910 that follows focuses on creating interpenetrating networks within the material.

Specifically, Ha et al., found that the use of trimethylolpropane trimethacrylate (TMPTMA) IPNs in VHB led to a decrease in viscoelasticity, higher mechanical efficiency, a high elastic strain energy density, and a high electromechanical coupling factor compared to unmodified 3 M VHB films [180,181]. The TMPTMA cross-links within the original polymer, forming networks that effectively freeze the pre-stretch in place, eliminating the need for external support. Characterization research conducted by Sahu et al., suggests that interpenetration decreases or eliminates the dependence on pre-stretching the material [182]. The authors found that cross-linking leads to a higher Young's modulus, which, as discussed in Section 3, leads to a decrease in actuation performance.

More recent literature has applied these principles to elastomers other than VHB. Tan et al., reduced the dependency on pre-stretch by adjusting cross-linking density in polyurethane acrylate (PUA), rather than VHB [196]. By cross-linking the PUA with 5, 10, and 15% by mass of polar cross-linked poly(ethylene glycol) diacrylate, they reduced response times by 50% compared to unmodified PUA. They decreased the viscoelastic drift from 0.28 mm after 145 cycles to 0.09 mm. As in the cross-linked VHB study performed by [182], Young's modulus increased with the maximum elongation decreasing from 960% to 167%. The 167% is comparable to PDMS. Furthermore, because the cross-linker is polar, there is an increase in the dielectric permittivity, which decreases the operating voltage.

Yu et al., implemented an ionic and silicone interpenetrating network by mixing amine-functional PDMS with carboxylic acid-functional PDMS to form an ionic network, and then mixing in commercial two-component silicone rubbers [197]. There was a 3 to 1000× increase of dielectric permittivity compared to the commercial elastomer at 0.1 MHz (depending on the commercial elastomer compared), and a more modest 1.5 to 2× increase at 1 MHz.

Rather than interpenetration on the molecular level, Xu et al., formed a self-healing dielectric elastomer using a liquid-solid interpenetration matrix [184]. They formed a porous silicone foam and filled it with hydroxyl silicone oil. This modification eliminated the need for pre-stretching, and the hydroxyl silicone oil can repair any dielectric breakdown in the silicone film.

5.2. Treatments to Achieve Self-Healing

Different levels of self-healing attributes have been achieved using various techniques. Using a thermoplastic methyl thioglycolate-modified styrene-butadiene-styrene (MGSBS) dielectric elastomer, Zhang et al. [198] achieved elastomers that could recover 67% of the initial dielectric strength after dielectric breakdown and 39% of initial dielectric strength after mechanical breakdown. Sun et al., formed self-healing silicone dielectric elastomers by combining PMS-g-COOH and PDMS-NH₂. At 80 °C, the polymer chains of PDMS-NH₂ rearrange and fill damaged areas by reforming hydrogen bonds. At 100 °C, the same mechanism occurs, except for the polymer chains of PMS-g-COOH and PDMS-NH₂ and

the interaction between COOH and NH_2 leads to an increase in ionic bonds. As ionic bonds are stronger than hydrogen bonds, at $100\text{ }^\circ\text{C}$, the elastomer achieves 115% of its original strength at the cost of a decrease in elastic modulus. Self-healing at $80\text{ }^\circ\text{C}$ can achieve 100% of its original strength without a decrease in elastic modulus. Both levels of self-healing are useful in different applications, and increased research in this area shows promise.

It is important to note that VHB 4910 has intrinsic self-healing properties. Fan and Szpunar characterized the self-healing ability of VHB 4910 by Raman spectrum analysis of cut interfaces on the material [199]. As Raman spectroscopy measures chemical bonds, the researchers measured the increase in Raman spectrum intensity over time. They found 44% recovery after 10 min and 95% recovery after 240 min. At elevated temperatures, healed VHB 4910 can have even higher mechanical strength than the original samples, achieving 120% efficiency after being heated for 120 min at $120\text{ }^\circ\text{C}$. The researchers attributed the self-healing ability to hydrophobic associations and hydrogen bonding that joined separated carbonyl group and hydroxyl group chains. This self-healing ability can greatly extend the lifetime of DEAs. Interested readers are directed to further reviews on self-healing elastomers in references [185,186].

5.3. Addition of Fillers

As discussed previously, pre-stretching and variation of cross-linking density are two common methods to reduce electromechanical instabilities, which in turn lead to increases in Young's modulus. For materials such as VHB and PUA, with inherently low Young's moduli but low dielectric breakdown strength [179,200], reducing electromechanical instabilities is of greater value than decreasing Young's modulus. In contrast, silicone elastomers have excellent dielectric strength and lower viscous losses than acrylic elastomers [201]. However, they require significantly higher operating voltages than other materials as a result of their low dielectric constants. Thus, most chemical modifications applied to silicone elastomers focus on increasing the dielectric constant and reducing Young's modulus.

One method of increasing the dielectric constant is by adding fillers [179,189]. Zhang et al., increased the dielectric constant of a commercial, mold-cast silicone elastomer [189] by adding BaTiO_3 particles (with a dielectric constant greater than 3000). Their results showed that an increase in the concentration of BaTiO_3 particles increased the dielectric constant of the composite. However, the elastic modulus increased and the breakdown voltage decreased with an increase in particle concentration, which negatively affected the actuation performance. Bortot et al., also focused on the introduction of ceramics in silicone elastomers, specifically focusing on DEGs [187]. They focused on creating a DEG composite, notably one with ferroelectric ceramic particles: lead magnesium niobate–lead titanate (PMN-PT) and lead zirconate-titanate (PZT) embedded in a silicone dielectric elastomer, polydimethylsiloxane (PDMS). Both improved the permittivity with respect to the unmodified silicone, although the stiffness increased and the electric breakdown strength decreased. Neglecting losses, the PMN-PT composite gave gains of up to 63% in energy per unit volume for silicone, while the PZT gave gains of up to 37%.

5.4. Blending with Another Polymer

Blending, which typically involves the combination of two or more types of polymers—rather than the addition of particles—can be more advantageous in some aspects [201]. For example, while composites with fillers could lead to dielectric losses and thus low dielectric strength [202], blending could provide a solution to this problem. For instance, Gallone et al., blended polyurethane (PU) and polydimethylsiloxane (PDMS) rather than adding conductive or ceramic fillers. They compared its effectiveness to traditional composites [188] and found blending polymeric phases to be more effective. Zhang et al., created a blend by UV curing polymethylvinylsiloxane with different doses of 2,2'-(ethylenedioxy)diethanethiol [203]. Unlike modifications of acrylic and PU which increased cross-link density, they reduced the density to achieve a macromolecular network with a low elastic modulus to enhance the actuation strain of elastomers.

They accomplished this with a high molecular weight of polymethylvinylsiloxane and a low dose of cross-linker. This led to a long chain length and low cross-link density, which gave the elastomer a low elastic modulus. There were soft but tough networks with poor cross-links, many entanglements, and few defects. Because of the lack of defects, low dielectric loss, and low conductivity of the material, Zhang et al., hypothesized that the modified material could have better electromechanical stability in comparison to unmodified polymethylvinylsiloxane.

Tugui et al., also made efforts to decrease Young's modulus and increase the dielectric permittivity via a blend [183]. They semi-interpenetrated polydimethylsiloxane (PDMS) with polyimides (PIs), creating a flexible backbone elastomer grafted with polarizable moieties. The researchers first attempted to incorporate polyamic acid (PAA-1) into PDMS but found the results to have poor mechanical properties due to large differences in material polarity. Poly(siloxane-imide) having carbon–nitrogen groups (PICOSI-1) was compatible because it had a more similar polarity.

The samples then stabilized, where it was assumed that some of the cross-linking reactions remained entangled in the chains, which caused a semi-interpenetrating network as opposed to a fully interpenetrating network. In the end, the more rigid polyimide chains led to significant improvements in dielectric properties and breakdown strength (possibly due to a synergistic effect between components) in all cases where weight percentages of polyimides greater than 2% were incorporated.

Mazurek et al., used liquid fillers to increase the permittivity of the dielectric elastomer. Specifically, liquid glycerol droplets were used, which enhanced the dielectric constant of the elastomer, while also serving as a softener, which decreased the elastic modulus of the elastomer. Increasing the glycerol concentration increases the droplet concentration without changing the droplet size until a threshold concentration is reached and a glycerol channel network is obtained instead of discrete droplets.

5.5. Polar Grafting

Unlike Zhang et al. [203] and Tugui et al. [183] who focused on blending and other work that introduced composites [187,192], Yang et al., introduced polar groups into a polymer [204]. The polar ester groups they introduced have excellent internal rotation ability, leading to a low glass transition temperature and therefore a low Young's modulus, while the polar nature of these groups leads to a high dielectric constant. They did not use silicone but instead produced an elastomer by polycondensation of 1,4-butanediol, 1,3-propanediol, sebacic acid, succinic acid, and itaconic acid. The resulting dielectric constant was higher than that of VHB 4910. Borayek et al., produced UV-printable dielectric elastomers rich in C=O and O–H polar groups by mixing hydroxypropyl acrylate, varying the ratios of diethylene glycol, photoinitiators, and light absorbers to allow UV printability. They achieved a dielectric constant 13 times that of VHB 4910 with a 30% increase in Young's modulus.

Polar grafting generally involves carboxyl (COOH), hydroxyl (OH), and ester (COOCH₃) groups and is on the angstrom scale [205]. The fillers used in composites vary in size from 1 nm (nanofillers) [206] to 2 μm barium titanite fillers [207]. Blends involve mixing different polymers, such as SEBS and PU [208] or nitrile rubber and thermoplastic polyurethane [209].

6. Controls

In the sequel, we present two paradigms for (modeling and) controls of soft actuators: (1) the traditional control paradigm, which is well described in the literature, and (2) a more adaptive control paradigm, which can make use of machine learning and rewritable hardware (e.g., FPGA), see Figure 4. A brief list of some of the methods referenced in this work, along with additional control strategies, is presented in Table 2.

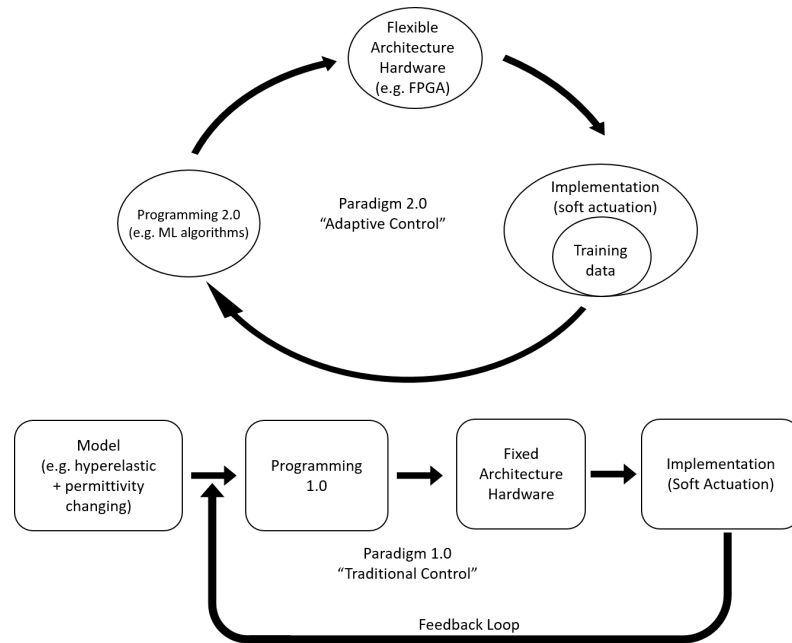


Figure 4. A visual representation of the two different paradigms utilized in modeling and controls. Below is paradigm 1.0 or traditional control, and above is paradigm 2.0, which can be viewed as an “adaptive control” scheme.

Table 2. A summary of some of the existing control methods for DEAs.

Control Method	Source
H_{∞}	[210]
ZIVS	[170]
LQR	[103]
Reinforcement Learning	[211,212]
Model Predictive Control	[213]
Two-step Forward Control	[214]

6.1. Traditional Control Techniques

Several methods have been used to control DEAs. Ye et al., used an H-infinity (H_{∞}) control scheme to create a conical dielectric elastomer actuator (CDEA) capable of small but accurate deformations [210]. The CDEA was used to replicate the changes in pressure that are felt when manually tracking an individual’s pulse. The H_{∞} controller accounted for noise in the system and was reported to perform better than a PID (proportional–integral–derivative) controller that was tuned using Matlab. Branz and Francesconi used a closed-loop transfer function-based control system to control the rotational displacement of an antagonistically coupled set of conical dielectric elastomer actuators [215]. The system relied on a set of dynamic simulations performed in Ansys to characterize the properties of the system. The transfer functions created from the simulations were used to map the measured and desired displacements to the required applied voltage.

Zou and Gu worked to create a control approach to minimize the impact of viscoelasticity on the actuation of a DEA [170]. They combined a feedforward controller with zero vibration input shaping (ZIVS) to create a creep compensator for a DEA. The controller used transfer functions determined experimentally using the Matlab Identification Toolbox. Gu et al., used a feedforward control to dynamically control small displacements to limit vibration in a DEA with an oscillating mass in the center [23].

By applying a finite-impulse-response (FIR) adaptive filter, Zhao et al., developed an active vibration controller that utilizes a filtered-x least-mean-square (Fx-LMS) algorithm to minimize vibrations of a conical system created by attaching a mass to the center of a DE membrane [34]. Mulembo et al., developed an LQR controller for μm displacements

of a DEA with solid carbon nanotube electrodes [103]. They combined an LQR controller with a Luenberger state observer for μm displacements in DEAs with solid electrodes. The DEAs utilized involved solid carbon nanotube electrodes. The work found that using an LQR controller having a Luenberger state observer was successful in mitigating the errors produced by the viscoelastic and nonlinear material properties. While the LQR controller was capable of producing accurate control of the DEA, the displacements were limited due to the solid electrodes involved with the design. Future work would involve extending the LQR controller to a design capable of achieving larger displacements.

6.2. Modern Control Techniques

Soft robots are usually more difficult to control than their conventional ‘stiff’ counterparts because of, in part, the higher degrees of freedom of the former. Drawing from the challenges of modeling highly nonlinear and time-dependent systems, several different research groups have utilized techniques from the field of modern control theory such as H_∞ -based controls [210], feedforward control [23], and inverse gray-box model-based control [26]. In general, the aforementioned techniques have been limited to applications that involve short ranges of actuation. Furthermore, various other factors such as the effects of deformation-dependent permittivity, temperature, humidity, and other operating conditions could further restrict controllability based on those techniques. Moreover, irregular geometries (as required for many soft robots) and electrode patterns could result in deformation states that are usually very difficult to express in closed form.

Lately, DEA researchers have tried to use data-based techniques to overcome the aforementioned challenges. In particular, reinforcement learning (RL) and deep reinforcement learning (DRL) have been exploited by some research groups [211,212]. In the sequel, we provide a brief overview of RL and a summary of some ML techniques that have been used in an attempt to more robustly control DEAs.

6.2.1. Introduction to Machine Learning

Reinforcement learning, along with supervised and unsupervised learning, constitutes fundamental machine learning models (see Figure 5). Rather than providing a direct classification, as in supervised learning, reinforcement learning determines the right balance between exploration and exploitation. Reinforcement learning instructs the system to learn an optimal policy—a deterministic mapping from time-state to action—by optimizing the reward provided by the environment over some time. Rewards are accumulated and tempered by a value function that specifies the expected reward of an action over time.

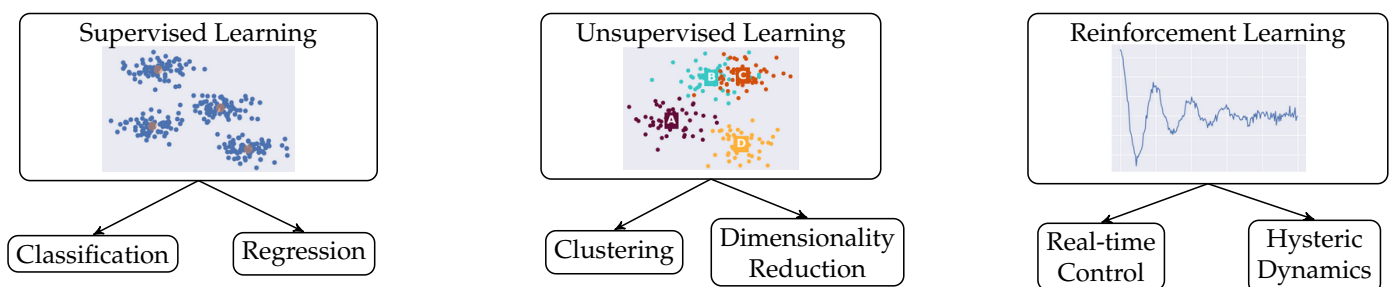


Figure 5. A comparative hierarchy of machine learning strategies. Techniques toward the left solve more difficult problems.

The environment of a reinforcement learning system is modeled as a Markov decision process (MDP). Described as a discrete-time control process, MDP allows modeling systems to have an agent whose decisions might be stochastically overridden by the environment. An MDP consists of a finite state space, \mathcal{S} , a finite action space, A , which gives the states reachable from state, s , a PMF (probability mass function), P_a , which gives the probability that taking action a in state s will leave the environment in state s' on the next timestep, and $R_a(s, s')$, the expected reward for a state change under action $a \in A$. A policy, $\pi(s)$,

is sought that provides the overall optimum action in state s . Once a policy is obtained, the action in state s is determined by the output of $\pi(s)$, and so the process reduces to a Markov chain, with the nice property of *memorylessness*, which simply means that the policy depends only on the current state.

Temporal difference learning is the most efficient form of learning for high-dimensional state data, a subclass that is Q -learning. The quality-value function (Q -function) maps a state, s , and action, a , to respective real parameter, or $Q : \mathcal{S} \times \mathcal{A} \rightarrow \mathbb{R}$. This mapping can occur via parameterization by a function approximator such as a neural network, or a more exotic choice, like a Gaussian mixture model. In a case like an explicit lookup table, the update rule can be expressed as follows:

$$\underbrace{Q(s_t, a_t)}_{\text{new value}} \leftarrow \underbrace{Q(s_t, a_t)}_{\text{old value}} + \underbrace{\alpha}_{\text{learning rate}} \cdot \underbrace{\left(\underbrace{r_t}_{\text{reward}} + \underbrace{\gamma}_{\text{discount factor}} \cdot \underbrace{\max_a Q(s_{t+1}, a)}_{\text{estimate of optimal future value}} - \underbrace{Q(s_t, a_t)}_{\text{old value}} \right)}_{\text{temporal difference}} \quad (17)$$

new value (temporal difference target)

where the index t is the current timestep, $a, a' \in \mathcal{A}$ and $s, s' \in \mathcal{S}$, and α is the *learning rate*. The *discount rate* γ weighs the old policy against the new policy.

When the Q -function is parameterized by a deep neural network, the learning system is called a *deep Q-network*. As the following section illustrates, deep Q -networks and deep reinforcement learning more generally have found applications in the controls of soft robotics [212].

6.2.2. Established Machine Learning for DEA Control

Model-based RL builds an internal representation (simulator) of the stochastic system and then finds a policy that optimizes the simulated system. Such a model consists of a transition probability distribution and a reward function over the Markov decision process. A model-based algorithm learns a model of the environment and then learns a policy based on its model. Thus, a model-based algorithm can plan ahead; it can consider future states before they are experienced. The model-free algorithms, however, learn strictly from trial and error; they do not know the impact a decision will have even one iteration further.

One of the seminal works on model-free neural network-based soft robotic control did not use reinforcement learning at all, but rather a control law based upon a PID controller [216]. Indeed, when the integral of the neural feedforward section is driven to zero, the controller acts as a traditional PID. This is quite similar to the model proposed in [217] for multiple-input, multiple-output systems. The goal is to bring the output tracking error down to zero as time progresses; thus, this technique implements semi-global asymptotic tracking control of the system. However, in this case, the feed-forward neural network does not require a robust model that accounts for the system's nonlinear dynamics. An experimentally tuned number of feedforward neurons under actuation provided a dramatic improvement in the tracking error over the traditional PID controller, without a feedforward component. Although there is interesting literature on machine learning for soft robotics more broadly [218], this section will discuss machine learning specifically for DEAs.

As illustrated in Figure 5, there are three fundamental models of machine learning: unsupervised, supervised, and reinforcement. Unsupervised learning can discern clustering in datasets, while supervised learning can perform classification. Reinforcement learning (RL), however, enables live control in a Markov decision process. Rather than providing a direct classification, as in supervised learning, RL determines the right balance of exploration and exploitation. This type learns an optimal *policy*—a deterministic mapping from time-state to action—by optimizing the reward provided by the environment over some time. As Figure 6 indicates, an agent sends actions to an actuator and receives the

actuator's new state. A value function, which specifies the expected reward of an action over time, accumulates and tempers rewards.

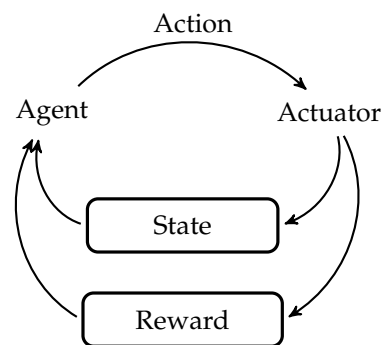


Figure 6. Reinforcement Learning.

Temporal difference learning methods, which form a subset of RL methods, are model-free. Model-free learning is desirable for elastomer control, since the high-dimensional and often continuous-time data would be difficult to simulate. However, because all learned information must be experimentally determined, reinforcement learning can require an unrealistically large test dataset. Using partial (inaccurate) models to speed up learning is another proposed approach [219]. To our knowledge, there have not been published applications of such a hybrid structure to DEA control. These areas should be considered prime areas for new research.

In [212], it was noted that, to the best of their knowledge, their work was the first to apply RL to even simple circular and rectangular DEAs. Thus, this article presents the current primary authority on machine learning control for DEAs (The authors attempted to collect data to confirm those results, during the time of the COVID-19 pandemic [220]). RL was used to precisely control such a planar DEA in randomly generated sine, triangle, and square waves over extended epochs of 45 s. For control, *Q*-learning—a specialization of temporal difference learning—was used. The method is called *deep Q*-learning because the *Q*-function is parameterized by a neural network [221]. It is the update rule that distinguishes *Q*-learning. Model-free learning is achieved by first starting with a fourth-order polynomial approximation of the desired displacement against the required voltage at each time step under modeling. A time step of 0.1 s proves sufficient for simulating continuous control. Unlike in [222], machine learning is used to fine-tune an already good approximation. A multilayer perceptron with two hidden layers is used as the *Q*-function. The impacts of reinforcement learning were especially pronounced in a rectangular DEA, where the reinforcement learning controller had a root mean squared error of about half that given by a traditional PID controller. Moreover, the PI controller had been manually adjusted, but the RL agent learned all it needed in the training phase. Moreover, the same training data could still accurately control an elastomer on the second day, when aging would have changed many of its characteristics.

A simple deep *Q*-network sufficed for a short control period over a relatively good approximation, but from scratch learning over longer time intervals requires two important refinements. First, note that many experimental setups do not explicitly measure velocity information; they rely solely upon an optical sensor to measure elastomer displacement at any instant. Accurately controlling the elastomer requires some memory over time, because the dynamics of the process are only partially observable. Indeed, the hysteresis means that the controller state space is not truly Markovian [222]. A solution could be forced by ensuring that the network keeps a fixed number of past states in memory, but this does not provide long-term planning or optimize memory usage [223]. However, there is a single solution to these problems: the deep recurrent *Q*-network (DRQN) [224].

Originally developed for state-dependent and flickered-screen Atari games, a DRQN incorporates a recurrent neural network (RNN) rather than a standard feedforward network.

These recurring networks maintain a hidden and time-dependent state that contextualizes new information [225,226], making them useful for linguistic analysis and control applications. However, raw RNNs themselves have several problems, including the infamous vanishing gradient problem. Thus, they are generally presented as long-short-term memory (LSTM) or gated recurrent unit (GRU) networks to appropriately control learning.

Note, however, that DRQN is not the only approach for partially observable or otherwise non-Markovian control. Other temporal difference methods, like actor-critic (AC), have proven useful for solving environments like the partially observable cart-pole problem [223]. Ideas like DRQN have found application in robotic vision feedback [227], and LSTM networks have found success in learning inverse dynamics for a rigid robot far more efficiently than the Gaussian regression model [228]. In [229], sensors embedded in an arbitrary soft actuator can have dynamics analyzed via an LSTM network.

The hysteretic recurrent neural network (HRNN) learns hysteretic behavior by viewing the Preisach curve as two sigmoid activation functions [230], with conservative neuron usage and standard training techniques. By allowing the agent to dynamically learn which information is most important to remember under the reward function, DRQNs resolve the prior partial observability and Markovian issues. [231] applies long short-term memory (LSTM) modeling to a Hammerstein–Wiener nonlinear system. There exists well-developed literature that applies recurrence and partial observability to control problems [232].

Other authors emphasize experience replay [211,233], an important feature of the RL used in [212]. The authors present an artificial muscle, designed to propel itself through the water in jets like a cuttlefish. Energized DEAs draw water into the swim bladder; with a swift reverse of the actuation, the water would be expelled and the robot would move forward. The authors employed a particularly simple deep-RL method: They used just two possible states—full voltage and no voltage—with a replay memory. Each entry in the replay memory is a 4-tuple (s_t, a_t, r_t, s_{t+1}) , called the *experience*, where t is the current timestep, s is the state, a is the action, and r is the reward. Up to some memory limit, each experience is stored in the replay memory to train the neural network that parameterizes the Q -function. To avoid a bias of correlation, the samples are chosen randomly from memory. Thus, computationally expensive training of the Q -function network can occur when live control is not happening. The Q -table, however, is continually updated. Epsilon-greedy learning was also used to guarantee exploratory behavior, and the reward function was designed to emphasize significant displacement with each actuation. Moreover, by fixing the number of timesteps per episode, the robot's learning progress could be measured by how far it swam in that allotted time. From the first episode to the 23rd episode, the authors saw an increase in average velocity of 91% with the binary action space.

In [234], reinforcement learning is not used for control, but for measurement of high-dimensional deformation. Here, the dielectric material functions as an array of stretchable capacitors arranged as a hemispheroid. Similar nonlinear effects occur here; it is well-known that as elastomers are stretched, the dielectric permittivity decreases. However, measuring relative deformation rather than trying to map a specific image from sensor data puts this task in the domain of neural networks. The learning task is to recognize gestures with sufficient real-time sampling resolution (10 Hz) to control a game of Tetris, as well as detect users by their gestures. Reinforcement learning is not used at all, but rather convolutional neural networks (CNNs) generate a feature map from the bitmap actuation data. To recognize gestures, a 3D CNN is used to take sensor input to a distribution over the gesture space. "Touch localization" uses a 2D version of the same network. A sampling rate of 10Hz allows the system to respond to input in 100 ms. The trained model could recognize one of 10 individual users by their gestures about 98% of the time. A generalized approach to accurate sensing even in non-linear soft sensors is the focus of [229].

6.2.3. Further Investigations into Machine Learning

Recent research into physics-informed neural networks (PINNs) [235] shows promise for another control strategy for DEAs. Similarly to [219], PINNs would reduce the expe-

rience required for adequate training. However, the learning strategy described in [235] is supervised, whereas control problems are inherently unsupervised. Therefore, one of the most open areas for DEA control research is the development of general machine learning strategies. Recall that the controller in [212] used a discrete action space of size 21. To our knowledge, even though Q -learning in continuous action spaces has been well established [236], no published studies have analyzed control performance in continuous action spaces.

Further research would also compare Q -learning with the SARSA (state–action–reward–state–action) method. [222] declared SARSA preferable to Q -learning for controlling a shape-memory alloy, which exhibits highly hysteretic behavior similar to DEAs.

7. Field-Programmable Gate Arrays for Control Applications

7.1. Introduction to FPGAs

The current paradigm of software and hardware interactions relies on rigid architectures and components. However, as new approaches to computing involve machine learning and soft robotics, there is a need to implement more flexible or reconfigurable hardware (see Figure 7). Field-programmable gate arrays (FPGAs) usage with DEA has been mainly focused on control systems with feedback response [25,237,238]. With new developments in AI research and FPGA topography, there has been a push to incorporate both technologies to create an accelerator for Artificial Neural Networks (ANN) [239–243].

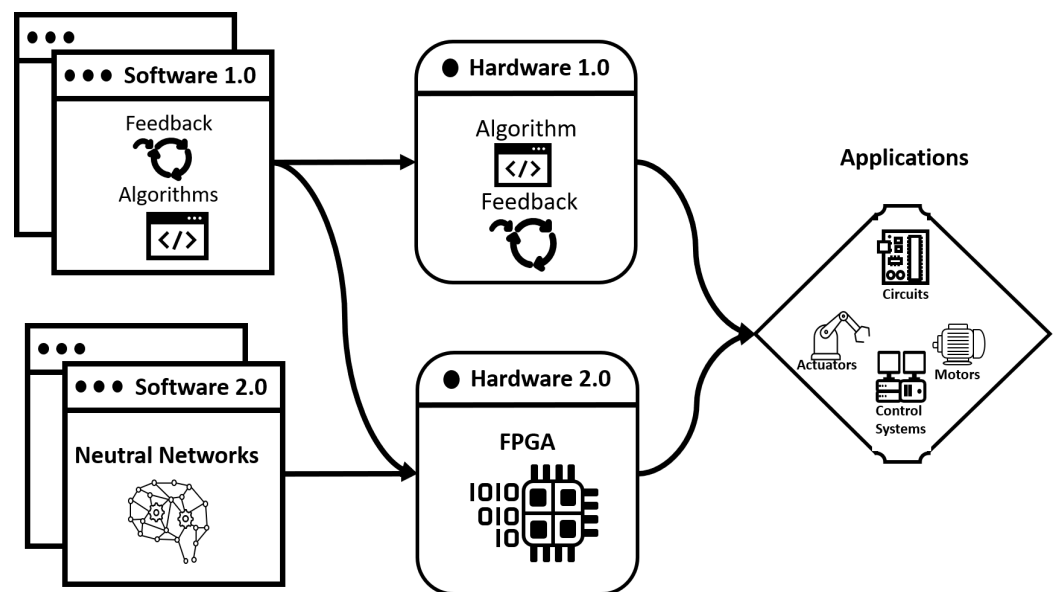


Figure 7. The current paradigm of software and hardware interactions (Software 1.0 and Hardware 1.0) relies on rigid architectures and components. With new approaches to computing—involving machine learning and soft robotics—hardware and software implementations are becoming more flexible (Software 2.0 and Hardware 2.0).

FPGA has unique properties that can be used to accelerate ANN. FPGAs are integrated circuits capable of converting digital functions into circuitry onto the silicon itself. FPGAs have many features found in a current system on a chip (SoC); these features include co-processors, networking, memory, phase-locked loops (PLL), USB control, and multipliers [244]. Along with these features, the current FPGA can also be reconfigured on the fly. This feature, called run-time reconfiguration (RTR), allows the FPGA system to automatically adjust to its surroundings in the field [245–247]. FPGAs differ from common processing options such as application-specific integrated circuits (ASICs) and microprocessors by allowing the circuitry to be reprogrammed directly to suit the application [240,243]. Reconfiguring RTR requires specialized knowledge with different FPGA manufacturers having different tool chains to implement the RTR feature [246,247]. In addition, FPGAs

tend to be more flexible in overall design, maintain a lower cost, and allow for the alteration of circuitry after manufacturing [239,247,248]. A major interest in FPGA technology comes from control systems that are built using intellectual property (IP) ASIC.

Future research is needed on optimizing the implementation of RTR onto existing core-based IP modules (e.g., motor controller) for FPGA. Specifically, research could focus on RTR module design so that modules can be dynamically replaced. The resulting system allows the FPGA to be independently managed through the use of its embedded coprocessor [245]. Due to the limitations of RTR, another area of future research could be the expansion of the sectors of the FPGA that it can reconfigure [244,248].

7.2. Control Applications with FPGAs

For some DEA configurations, customized controllers are required. The flexibility of FPGA makes it very useful in these types of applications, as they can be customized to meet the desired DEA control. In addition, high-speed sampling can be achieved with FPGAs, with reported solutions capable of sampling 20,000 times a second [238]. Thus, FPGAs can be used to control and monitor DEA deformation experiments, serving as a tool for high-speed data collection, while maintaining the ability to record data from multiple sources. An example of this would be the monitoring of various properties of a DE-based device, such as force-displacement, deformation, capacitance, and resistance [249]. Another area of future research is finding ways to reduce the resistive effects that come from the high-frequency samplings of DEA. The resistive effects will need to be factored into the FPGA control signal to the DEA [75].

The FPGA, comprised of multiple individual internal components, supports numerous communication protocols and exhibits modularity [245,250]. This latter property allows the FPGA to be configured as individual modules and subsystems [251]. Based on this modularity, the coprocessor subsystem can be configured to handle the computational processes, while the other individual modules can be programmed to handle all external control and communication. The internal co-processor can run a real-time operating system (RTOS), this allows for rapid prototyping of filtering algorithms in real time. This can be very useful when controlling soft actuators that require simultaneously complex computations and data collection. An example of this was implemented by [237] to control a soft pneumatic actuator (SPA). It was carried out using an NI CompactRIO[®] real-time controller and coded using the NI LabView[®] software. The FPGA was set to run at 40 MHz, and the RTOS co-processor running at 1 MHz. The resulting system was able to accurately drive the SPAs with a mean absolute error of 2.34 mm/s (extension) and 1.70 mm/s (contraction) at 100 kPa pressure.

FPGAs can be used to enhance existing systems by integration or substitution, allowing them to exhibit more features [252]. Various implementations of this were developed by [250]. For example, they used a digital signal processor (DSP) as the central controller with multiple FPGAs handling the different transmission lines. (It might be worth noting that the intercommunication for the digital controllers was handled through fiber-optic links using synchronous serial for high-speed communication of 9.375 Mb/s between the DPS and FPGA.) In the modified version of the aforementioned, they also used a DSP as the central controller with multiple FPGAs and other slave DSPs handling the individual transmission lines. In addition, FPGA could enhance existing systems by completely substituting them. An example of this was also implemented by [250]. In a data handling application, they reported using an FPGA to handle the different communications in a flexible AC transmission system (FACTS).

Another potential use for FPGA nominated by [252] would involve a vision-based tactile sensing system. In that application, the FPGA can be incorporated to boost the speed of image processing algorithms or even, perhaps, provide machine learning capabilities to the embedded system. Granted, more research is needed on the different ways to incorporate FPGAs into existing systems which can lead to increased redundancy and reduce cost [250].

7.3. Implementation

The implementation of machine learning on FPGA can be achieved in different ways. Several researchers use FPGA lookup tables [248]. Others use hybrid systems, where machine learning is offloaded onto the embedded processor [253]. There is some interest in using the RTR properties of the FPGA with the so-called digital spiking neural network (SNN). With an interest in creating analog and digital spiking neural networks (SNNs) [254], Upegui et al. [255] proposed a digital SNN system, which they created on a Spartan II xc2s200 FPGA. The system was comprised of three parts, a hardware substrate, a computation engine, and an adaptation mechanism. The resulting system was able to handle 30 neurons and achieved time slices of only 64 clock cycles with an operating frequency of 54.4 MHz. In addition to speed benefits, the implementation of such systems could help solve problems that possess such complexities that they require varying architectures.

The use of FPGAs as an accelerator of more traditional ML-based systems is another area of research. One benefit is that you can produce faster model-free reinforcement learning. The main drive of such research stems from the need for autonomous robotic systems for space exploration, allowing the system to self-react to its current situation. A proposed system done by [253] with a Xilinx Virtex7 FPGA was able to achieve a 12.12 microsecond update time for their Q-values while operating at 20 Watts compared to needing 2612.24 microseconds to update the Q-values on a 2.3 GHz CPU.

Another expanding area of FPGA research is its application in hybrid fuzzy logic controllers (FLCs). Fuzzy logic is a mathematical framework that addresses the uncertainty and imprecision characteristic of human reasoning. Its primary advantage lies in simplifying complex systems into basic IF–THEN rules. These IF–THEN blocks can be implemented on individual FPGA modules, enabling rapid prototyping and cost-effective implementation of FLCs [239].

Further research is needed to optimize the resources available on existing FPGA. The limited look-up tables (LUTs) and logic elements on existing FPGA chip sets allow a small neural network to be created [255]. Research is being conducted on using a coordinate rotation digital computer (CORDIC) approach with the RTR property of FPGAs [253]. By repurposing components of the FPGA not being utilized for computations, the CORDIC approach aims to increase the number of neurons in a machine learning program on an FPGA. The end goal of utilizing both the general-purpose processing system on the FPGA and the software-assigned task is to provide increased speed for fuzzy logic computations [239].

8. Conclusions

Soft robotics are of great interest to researchers and developers due to their potential for biomimetic applications across a myriad of fields, including biomedicine (e.g., surgery and endoscopy), the film industry (e.g., animatronics), ecology (e.g., physical ‘animats’), human–robot interactions (e.g., social robots), and others. In contrast to their rigid counterparts, soft robotics offer obvious actuation benefits, including their many degrees of freedom in motion and their potential to mimic living organisms. Of course, critical to the advancement of soft robotics is the successful development of soft actuators, which can involve many challenges. This review focused on DEAs and included the applications, modeling, material challenges and solutions, and control of DEAS. In addition, more modern control schemes, such as reinforcement learning and adaptive controller hardware, such as FPGAs, were reviewed. In contrast to other reviews, the current work aims to (1) provide non-experts with an “easy-to-follow” survey of the various aspects and challenges to consider when implementing DE-based soft actuators, and (2) highlight current solutions and challenges related to the controls and portability of DE-based soft-robotic systems. The development of computational tools to assist the designer is needed. For example, the consolidation of the dozens of hyperelastic material models in a ‘ready-to-compute’ form could be very beneficial, especially to non-experts in the field of soft robotics.

Author Contributions: Conceptualization, H.M.; methodology, H.M.; validation, H.M., C.F. and I.L.; formal analysis, H.M. and C.F.; investigation, H.M., C.F. and I.L.; writing—original draft preparation, H.M., C.F. and I.L.; writing—review and editing, H.M. and C.F.; visualization, C.F. and I.L.; supervision, H.M.; project administration, H.M. All authors have read and agreed to the published version of the manuscript.

Funding: This research received no external funding.

Acknowledgments: The authors would like to thank the Center for Research and Scholarship at Liberty University for their support of our research.

Conflicts of Interest: The authors declare no conflicts of interest or any other ethical issue.

References

- Pfeil, S.; Henke, M.; Katzer, K.; Zimmermann, M.; Gerlach, G. A Worm-Like Biomimetic Crawling Robot Based on Cylindrical Dielectric Elastomer Actuators. *Front. Robot. AI* **2020**, *7*, 9. [[CrossRef](#)] [[PubMed](#)]
- Minaminosono, A.; Shigemune, H.; Okuno, Y.; Katsumata, T.; Hosoya, N.; Maeda, S. A deformable motor driven by dielectric elastomer actuators and flexible mechanisms. *Front. Robot. AI* **2019**, *6*, 1. [[CrossRef](#)] [[PubMed](#)]
- Christianson, C.; Goldberg, N.N.; Deheyn, D.D.; Cai, S.; Tolley, M.T. Translucent soft robots driven by frameless fluid electrode dielectric elastomer actuators. *Sci. Robot.* **2018**, *3*, eaat1893
- Nguyen, C.T.; Phung, H.; Nguyen, T.D.; Jung, H.; Choi, H.R. Multiple-degrees-of-freedom dielectric elastomer actuators for soft printable hexapod robot. *Sens. Actuators A Phys.* **2017**, *267*, 505–516. [[CrossRef](#)]
- Duduta, M.; Clarke, D.R.; Wood, R.J. A high speed soft robot based on dielectric elastomer actuators. In Proceedings of the 2017 IEEE International Conference on Robotics and Automation (ICRA), Singapore, 29 May–3 June 2017; IEEE: Piscataway, NJ, USA, 2017; pp. 4346–4351.
- Wang, N.; Guo, H.; Chen, B.; Cui, C.; Zhang, X. Design of dielectric elastomer actuator using topology optimization method based on genetic algorithm. *Smart Mater. Struct.* **2019**, *28*, 065013. [[CrossRef](#)]
- Park, B.J.; Park, S.; Choi, M.; Park, S.K.; Yun, S.; Shin, E.; Yoon, J.W. Monolithic focus-tunable lens technology enabled by disk-type dielectric-elastomer actuators. *Sci. Rep.* **2020**, *10*, 16937. [[CrossRef](#)] [[PubMed](#)]
- Hajiesmaili, E.; Clarke, D.R. Reconfigurable shape-morphing dielectric elastomers using spatially varying electric fields. *Nat. Commun.* **2019**, *10*, 183. [[CrossRef](#)]
- Shian, S.; Diebold, R.M.; Clarke, D.R. Tunable lenses using transparent dielectric elastomer actuators. *Opt. Express* **2013**, *21*, 8669–8676. [[CrossRef](#)] [[PubMed](#)]
- Nam, S.; Yun, S.; Yoon, J.W.; Park, S.; Park, S.K.; Mun, S.; Park, B.; Kyung, K.U. A robust soft lens for tunable camera application using dielectric elastomer actuators. *Soft Robot.* **2018**, *5*, 777–782. [[CrossRef](#)]
- Daheshpour, K.; Mazlouman, S.J.; Mahanfar, A.; Yun, J.X.; Han, X.; Menon, C.; Carpi, F.; Vaughan, R.G. Pattern reconfigurable antenna based on moving V-shaped parasitic elements actuated by dielectric elastomer. *Electron. Lett.* **2010**, *46*, 886–888. [[CrossRef](#)]
- Mazlouman, S.J.; Soleimani, M.; Mahanfar, A.; Menon, C.; Vaughan, R.G. Pattern reconfigurable square ring patch antenna actuated by hemispherical dielectric elastomer. *Electron. Lett.* **2011**, *47*, 164–165. [[CrossRef](#)]
- Gent, A.N. A new constitutive relation for rubber. *Rubber Chem. Technol.* **1996**, *69*, 59–61. [[CrossRef](#)]
- Treloar, L. The elasticity of a network of long-chain molecules. I. *Trans. Faraday Soc.* **1943**, *39*, 36–41. [[CrossRef](#)]
- Zhao, X.; Koh, S.J.A.; Suo, Z. Nonequilibrium thermodynamics of dielectric elastomers. *Int. J. Appl. Mech.* **2011**, *3*, 203–217. [[CrossRef](#)]
- Xiang, Y.; Zhong, D.; Wang, P.; Yin, T.; Zhou, H.; Yu, H.; Baliga, C.; Qu, S.; Yang, W. A physically based visco-hyperelastic constitutive model for soft materials. *J. Mech. Phys. Solids* **2019**, *128*, 208–218. [[CrossRef](#)]
- Zhang, J.; Ru, J.; Chen, H.; Li, D.; Lu, J. Viscoelastic creep and relaxation of dielectric elastomers characterized by a Kelvin-Voigt-Maxwell model. *Appl. Phys. Lett.* **2017**, *110*, 044104. [[CrossRef](#)]
- Jiménez, S.M.; McMeeking, R.M. Deformation dependent dielectric permittivity and its effect on actuator performance and stability. *Int. J. Non-Linear Mech.* **2013**, *57*, 183–191. [[CrossRef](#)]
- Jiménez, S.M.; McMeeking, R.M. A constitutive law for dielectric elastomers subject to high levels of stretch during combined electrostatic and mechanical loading: Elastomer stiffening and deformation dependent dielectric permittivity. *Int. J. Non-Linear Mech.* **2016**, *87*, 125–136. [[CrossRef](#)]
- Farmer, C.; Medina, H. Effects of electrostriction on the bifurcated electro-mechanical performance of conical dielectric elastomer actuators and sensors. *Robotica* **2023**, *41*, 215–235. [[CrossRef](#)]
- Pu, J.; Meng, Y.; Xie, Z.; Peng, Z.; Wu, J.; Shi, Y.; Plamthottam, R.; Yang, W.; Pei, Q. A unimorph nanocomposite dielectric elastomer for large out-of-plane actuation. *Sci. Adv.* **2022**, *8*, eabm6200. [[CrossRef](#)]
- Wang, Y.; Kim, S.; Li, G.; Sun, L. Filler orientation effect on relative permittivity of dielectric elastomer nanocomposites filled with carbon nanotubes. *Comput. Mater. Sci.* **2015**, *104*, 69–75. [[CrossRef](#)]

23. Gu, G.Y.; Gupta, U.; Zhu, J.; Zhu, L.M.; Zhu, X.Y. Feedforward deformation control of a dielectric elastomer actuator based on a nonlinear dynamic model. *Appl. Phys. Lett.* **2015**, *107*, 042907. [[CrossRef](#)]
24. Kelley, C.R.; Kauffman, J.L. Tremor suppression controller for dielectric elastomer orthosis. In Proceedings of the Electroactive Polymer Actuators and Devices (EAPAD) XX, Denver, CO, USA, 5–8 March 2018; International Society for Optics and Photonics: Bellingham, WA, USA, 2018; Volume 10594, p. 105940U.
25. Rizzello, G.; Naso, D.; York, A.; Seelecke, S. Closed loop control of dielectric elastomer actuators based on self-sensing displacement feedback. *Smart Mater. Struct.* **2016**, *25*, 035034. [[CrossRef](#)]
26. Jones, R.W.; Sarban, R. Inverse grey-box model-based control of a dielectric elastomer actuator. *Smart Mater. Struct.* **2012**, *21*, 075019. [[CrossRef](#)]
27. Hoffstadt, T.; Maas, J. Model-based self-sensing algorithm for dielectric elastomer transducers based on an extended Kalman filter. *Mechatronics* **2018**, *50*, 248–258. [[CrossRef](#)]
28. Gu, G.Y.; Zhu, J.; Zhu, L.M.; Zhu, X. A survey on dielectric elastomer actuators for soft robots. *Bioinspiration Biomim.* **2017**, *12*, 011003. [[CrossRef](#)]
29. Gupta, U.; Qin, L.; Wang, Y.; Godaba, H.; Zhu, J. Soft robots based on dielectric elastomer actuators: A review. *Smart Mater. Struct.* **2019**, *28*, 103002. [[CrossRef](#)]
30. Youn, J.H.; Jeong, S.M.; Hwang, G.; Kim, H.; Hyeon, K.; Park, J.; Kyung, K.U. Dielectric elastomer actuator for soft robotics applications and challenges. *Appl. Sci.* **2020**, *10*, 640. [[CrossRef](#)]
31. Wang, J.; Li, S.; Gao, D.; Xiong, J.; Lee, P.S. Reconfigurable and programmable origami dielectric elastomer actuators with 3D shape morphing and emissive architectures. *NPG Asia Mater.* **2019**, *11*, 71. [[CrossRef](#)]
32. Ashby, J.; Rosset, S.; Henke, E.F.M.; Anderson, I. Inflatable dielectric elastomer robots for space. In Proceedings of the Electroactive Polymer Actuators and Devices (EAPAD) XXI, Denver, CO, USA, 4–7 March 2019; International Society for Optics and Photonics: Bellingham, WA, USA, 2019; Volume 10966, p. 109661L.
33. Rossiter, J.; Conn, A.; Cerruto, A.; Winters, A.; Roke, C. Colour gamuts in polychromatic dielectric elastomer artificial chromophores. In Proceedings of the Electroactive Polymer Actuators and Devices (EAPAD), San Diego, CA, USA, 10–13 March 2014; International Society for Optics and Photonics: Bellingham, WA, USA, 2014; Volume 9056, p. 905620.
34. Zhao, Y.; Guo, Q.; Wu, S.; Meng, G.; Zhang, W. Design and experimental validation of an annular dielectric elastomer actuator for active vibration isolation. *Mech. Syst. Signal Process.* **2019**, *134*, 106367. [[CrossRef](#)]
35. Kornbluh, R.D.; Pelrine, R.; Pei, Q.; Heydt, R.; Stanford, S.; Oh, S.; Eckerle, J. Electroelastomers: Applications of dielectric elastomer transducers for actuation, generation, and smart structures. In Proceedings of the Smart Structures and Materials 2002: Industrial and Commercial Applications of Smart Structures Technologies, San Diego, CA, USA, 18–21 March 2002; International Society for Optics and Photonics: Bellingham, WA, USA, 2002; Volume 4698, pp. 254–270.
36. Waché, R.; McCarthy, D.N.; Risse, S.; Kofod, G. Rotary motion achieved by new torsional dielectric elastomer actuators design. *IEEE/ASME Trans. Mechatron.* **2014**, *20*, 975–977. [[CrossRef](#)]
37. Cao, C.; Burgess, S.; Conn, A.T. Toward a dielectric elastomer resonator driven flapping wing micro air vehicle. *Front. Robot. AI* **2019**, *5*, 137. [[CrossRef](#)] [[PubMed](#)]
38. Shintake, J.; Cacucciolo, V.; Shea, H.; Floreano, D. Soft biomimetic fish robot made of dielectric elastomer actuators. *Soft Robot.* **2018**, *5*, 466–474. [[CrossRef](#)] [[PubMed](#)]
39. Zhao, Z.; Shuai, C.; Gao, Y.; Rustighi, E.; An, Y. An application review of dielectric electroactive polymer actuators in acoustics and vibration control. In Proceedings of the Journal of Physics: Conference Series, Indore, India, 13–14 February 2016; Volume 744, p. 012162.
40. Lin, P.W.; Liu, C.H. Bio-inspired soft proboscis actuator driven by dielectric elastomer fluid transducers. *Polymers* **2019**, *11*, 142. [[CrossRef](#)] [[PubMed](#)]
41. Christianson, C.; Goldberg, N.N.; Tolley, M.T. Elastomeric diaphragm pump driven by fluid electrode dielectric elastomer actuators (FEDEAs). In Proceedings of the Electroactive Polymer Actuators and Devices (EAPAD) XX, Denver, CO, USA, 5–8 March 2018; International Society for Optics and Photonics: Bellingham, WA, USA, 2018; Volume 10594, p. 105940O.
42. Cho, K.H.; Kim, Y.; Yang, S.Y.; Kim, K.; Park, J.H.; Rodrigue, H.; Moon, H.; Koo, J.C.; Choi, H.R. Artificial musculoskeletal actuation module driven by twisted and coiled soft actuators. *Smart Mater. Struct.* **2019**, *28*, 125010. [[CrossRef](#)]
43. Choi, J.H.; Ahn, J.; Kim, J.B.; Kim, Y.C.; Lee, J.Y.; Oh, I.K. An electroactive, tunable, and frequency selective surface utilizing highly stretchable dielectric elastomer actuators based on functionally antagonistic aperture control. *Small* **2016**, *12*, 1840–1846. [[CrossRef](#)] [[PubMed](#)]
44. Kubo, M.; Li, X.; Kim, C.; Hashimoto, M.; Wiley, B.J.; Ham, D.; Whitesides, G.M. Stretchable microfluidic radiofrequency antennas. *Adv. Mater.* **2010**, *22*, 2749–2752. [[CrossRef](#)] [[PubMed](#)]
45. She, A.; Zhang, S.; Shian, S.; Clarke, D.R.; Capasso, F. Large Area Electrically Tunable Lenses Based on Metasurfaces and Dielectric Elastomer Actuators. *arXiv* **2017**, arXiv:1708.01972. <https://doi.org/10.48550/arXiv.1708.01972>.
46. Aschwanden, M.; Beck, M.; Stemmer, A. Diffractive transmission grating tuned by dielectric elastomer actuator. *IEEE Photonics Technol. Lett.* **2007**, *19*, 1090–1092. [[CrossRef](#)]
47. Wang, Q.; Wang, Z.Y.; Zhang, D.W.; Huang, Y.S.; Ni, Z.J.; Zhuang, S.L. Tunable guided-mode resonance filter based on dielectric elastomer actuators. *Optik* **2014**, *125*, 1990–1992. [[CrossRef](#)]

48. Lu, Z.; Godaba, H.; Cui, Y.; Foo, C.C.; Debiassi, M.; Zhu, J. An electronically tunable duct silencer using dielectric elastomer actuators. *J. Acoust. Soc. Am.* **2015**, *138*, EL236–EL241. [[CrossRef](#)] [[PubMed](#)]
49. Jia, K.; Wang, M.; Lu, T.; Zhang, J.; Wang, T. Band-gap tunable dielectric elastomer filter for low frequency noise. *Smart Mater. Struct.* **2016**, *25*, 055047. [[CrossRef](#)]
50. Zhang, R.; Lochmatter, P.; Kunz, A.; Kovacs, G.M. Spring roll dielectric elastomer actuators for a portable force feedback glove. In Proceedings of the Smart Structures and Materials 2006: Electroactive Polymer Actuators and Devices (EAPAD), San Diego, CA, USA, 26 February–2 March 2006; International Society for Optics and Photonics: Bellingham, WA, USA, 2006; Volume 6168, p. 61681T.
51. Opris, D.M.; Molberg, M.; Walder, C.; Ko, Y.S.; Fischer, B.; Nueesch, F.A. New silicone composites for dielectric elastomer actuator applications in competition with acrylic foil. *Adv. Funct. Mater.* **2011**, *21*, 3531–3539. [[CrossRef](#)]
52. Kanno, R.; Watanabe, S.; Shimizu, K.; Shintake, J. Self-sensing McKibben artificial muscles embedded with dielectric elastomer sensor. *IEEE Robot. Autom. Lett.* **2021**, *6*, 6274–6280. [[CrossRef](#)]
53. Zhu, Y.; Giffney, T.; Aw, K. A dielectric elastomer-based multimodal capacitive sensor. *Sensors* **2022**, *22*, 622. [[CrossRef](#)] [[PubMed](#)]
54. Nie, B.; Geng, J.; Yao, T.; Miao, Y.; Zhang, Y.; Chen, X.; Liu, J. Sensing arbitrary contact forces with a flexible porous dielectric elastomer. *Mater. Horiz.* **2021**, *8*, 962–971. [[CrossRef](#)]
55. Gratz-Kelly, S.; Krüger, T.; Rizzello, G.; Seelecke, S.; Moretti, G. An audio-tactile interface based on dielectric elastomer actuators. *Smart Mater. Struct.* **2023**, *32*, 034005. [[CrossRef](#)]
56. Ciarella, L.; Richter, A.; Henke, E.F.M. Integrated logic for dielectric elastomers: Replicating the reflex of the venus flytrap. *Adv. Mater. Technol.* **2023**, *8*, 2202000. [[CrossRef](#)]
57. Antillon, D.W.O.; Walker, C.; Rosset, S.; Anderson, I.A. The challenges of hand gesture recognition using dielectric elastomer sensors. In Proceedings of the Electroactive Polymer Actuators and Devices (EAPAD) XXII, Online, 27 April–8 May 2020; SPIE: Bellingham, WA, USA, 2020; Volume 11375, pp. 231–241.
58. Shrestha, M.; Lu, Z.; Lau, G.K. High humidity sensing by ‘hygromorphic’ dielectric elastomer actuator. *Sens. Actuators B Chem.* **2021**, *329*, 129268. [[CrossRef](#)]
59. Kornbluh, R.D.; Pelrine, R.; Prahlad, H.; Wong-Foy, A.; McCoy, B.; Kim, S.; Eckerle, J.; Low, T. Dielectric elastomers: Stretching the capabilities of energy harvesting. *MRS Bull.* **2012**, *37*, 246. [[CrossRef](#)]
60. Du, X.; Du, L.; Cai, X.; Hao, Z.; Xie, X.; Wu, F. Dielectric elastomer wave energy harvester with self-bias voltage of an ancillary wind generator to power for intelligent buoys. *Energy Convers. Manag.* **2022**, *253*, 115178. [[CrossRef](#)]
61. Zhang, C.; Lai, Z.; Zhang, G.; Yurchenko, D. Energy harvesting from a dynamic vibro-impact dielectric elastomer generator subjected to rotational excitations. *Nonlinear Dyn.* **2020**, *102*, 1271–1284. [[CrossRef](#)]
62. Zhang, C.; Lai, Z.; Li, M.; Yurchenko, D. Wind energy harvesting from a conventional turbine structure with an embedded vibro-impact dielectric elastomer generator. *J. Sound Vib.* **2020**, *487*, 115616. [[CrossRef](#)]
63. Vertechy, R.; Papini Rosati, G.P.; Fontana, M. Reduced model and application of inflating circular diaphragm dielectric elastomer generators for wave energy harvesting. *J. Vib. Acoust.* **2015**, *137*, 011004. [[CrossRef](#)]
64. Zhang, J.; Lai, Z.; Rao, X.; Zhang, C. Harvest rotational energy from a novel dielectric elastomer generator with crank-connecting rod mechanisms. *Smart Mater. Struct.* **2020**, *29*, 065005. [[CrossRef](#)]
65. Vertechy, R.; Fontana, M.; Papini, G.R.; Bergamasco, M. Oscillating-water-column wave-energy-converter based on dielectric elastomer generator. In Proceedings of the Electroactive Polymer Actuators and Devices (EAPAD), San Diego, CA, USA, 10–14 March 2013; International Society for Optics and Photonics: Bellingham, WA, USA, 2013; Volume 8687, p. 86870I.
66. Lai, H.; Reid, K. Investigation of dielectric elastomer human energy harvesting to reduce knee joint torque deviation due to bracing. *J. Rehabil. Assist. Technol. Eng.* **2019**, *6*, 1–9. [[CrossRef](#)]
67. Moretti, G.; Rosset, S.; Vertechy, R.; Anderson, I.; Fontana, M. A review of dielectric elastomer generator systems. *Adv. Intell. Syst.* **2020**, *2*, 2000125. [[CrossRef](#)]
68. Brochu, P.; Pei, Q., Dielectric elastomers for actuators and artificial muscles. In *Electroactivity in Polymeric Materials*; Rasmussen, L., Ed.; Springer: Boston, MA, USA, 2012; pp. 1–56. [[CrossRef](#)]
69. Jiabin, Z.; Weiping, Z.; Chenyang, W.; Yang, Z.; Jiahao, W. Current status of insect-inspired flapping wing micro air vehicles. In Proceedings of the 2019 IEEE International Conference on Unmanned Systems (ICUS), Beijing, China, 17–19 October 2019; pp. 894–898.
70. Pelrine, R.; Kornbluh, R.D.; Pei, Q.; Stanford, S.; Oh, S.; Eckerle, J.; Full, R.J.; Rosenthal, M.A.; Meijer, K. Dielectric elastomer artificial muscle actuators: Toward biomimetic motion. In Proceedings of the Smart Structures and Materials 2002: Electroactive Polymer Actuators and Devices (EAPAD), San Diego, CA, USA, 17–21 March 2002; International Society for Optics and Photonics: Bellingham, WA, USA 2002; Volume 4695, pp. 126–137.
71. Anderson, I.A.; Calius, E.P.; Gisby, T.; Hale, T.; McKay, T.; O’Brien, B.; Walbran, S. A dielectric elastomer actuator thin membrane rotary motor. In Proceedings of the Electroactive Polymer Actuators and Devices (EAPAD), San Diego, CA, USA, 8–12 March 2009; International Society for Optics and Photonics: Bellingham, WA, USA, 2009; Volume 7287, pp. 470–479. [[CrossRef](#)]
72. Sarban, R.; Jones, R.; Mace, B.; Rustighi, E. A tubular dielectric elastomer actuator: Fabrication, characterization and active vibration isolation. *Mech. Syst. Signal Process.* **2011**, *25*, 2879–2891. [[CrossRef](#)]
73. Kajiwara, I.; Kitabatake, S.; Hosoya, N.; Maeda, S. Design of dielectric elastomer actuators for vibration control at high frequencies. *Int. J. Mech. Sci.* **2019**, *157*, 849–857. [[CrossRef](#)]

74. Sarban, R.; Jones, R.W. Physical model-based active vibration control using a dielectric elastomer actuator. *J. Intell. Mater. Syst. Struct.* **2012**, *23*, 473–483. [[CrossRef](#)]
75. Sarban, R.; Jones, R.W. Electromechanical model-based vibration isolation using a dielectric elastomer actuator. In Proceedings of the 2011 IEEE International Conference on Mechatronics, Istanbul, Turkey, 13–15 April 2011; IEEE: Piscataway, NJ, USA, 2011; pp. 603–608.
76. Kelley, C.R.; Kauffman, J.L. Tremor-active controller for dielectric elastomer-based pathological tremor suppression. *IEEE/ASME Trans. Mechatron.* **2020**, *25*, 1143–1148. [[CrossRef](#)]
77. Kelley, C.R.; Kauffman, J.L. Necessary dielectric elastomer parameters for wearable tremor suppression. In Proceedings of the Electroactive Polymer Actuators and Devices (EAPAD) XXI, Denver, CO, USA, 4–7 March 2019; SPIE: Bellingham, WA, USA, 2019; Volume 10966, pp. 250–260.
78. Aksoy, B.; Shea, H. Reconfigurable and latching shape-morphing dielectric elastomers based on local stiffness modulation. *Adv. Funct. Mater.* **2020**, *30*, 2001597. [[CrossRef](#)]
79. Li, Y.; Gong, Z.; Zhang, T. Design Method of Minimum Energy Structural Dielectric Elastomer Actuators for Origami Robots. In Proceedings of the 2022 IEEE International Conference on Mechatronics and Automation (ICMA), Guilin, China, 7–10 August 2022; IEEE: Piscataway, NJ, USA, 2022; pp. 675–679.
80. Yin, X.; Zhou, P.; Wen, S.; Zhang, J. Origami Improved Dielectric Elastomer Actuation for Tunable Lens. *IEEE Trans. Instrum. Meas.* **2022**, *71*, 1–9. [[CrossRef](#)]
81. Zhao, P.; Cai, Y.; Liu, C.; Ge, D.; Li, B.; Chen, H. Study on the bio-inspired electrochromic device enabled via dielectric elastomer actuator. *Opt. Mater.* **2021**, *111*, 110569. [[CrossRef](#)]
82. Xiao, M.; Mao, J.; Kolloosche, M.; Hwang, V.; Clarke, D.R.; Manoharan, V.N. Voltage-tunable elastomer composites that use shape instabilities for rapid structural color changes. *Mater. Horiz.* **2022**, *9*, 1954–1961. [[CrossRef](#)] [[PubMed](#)]
83. Bauer, S.; Bauer-Gogonea, S.; Graz, I.; Kaltenbrunner, M.; Keplinger, C.; Schwödiauer, R. 25th anniversary article: A soft future: From robots and sensor skin to energy harvesters. *Adv. Mater.* **2014**, *26*, 149–162. [[CrossRef](#)] [[PubMed](#)]
84. Li, P.; Wang, Y.; Gupta, U.; Liu, J.; Zhang, L.; Du, D.; Foo, C.C.; Ouyang, J.; Zhu, J. Transparent soft robots for effective camouflage. *Adv. Funct. Mater.* **2019**, *29*, 1901908. [[CrossRef](#)]
85. Christodoulou, C.G.; Tawk, Y.; Lane, S.A.; Erwin, S.R. Reconfigurable antennas for wireless and space applications. *Proc. IEEE* **2012**, *100*, 2250–2261. [[CrossRef](#)]
86. Jiang, X.J.; Mazlouman, S.J.; Mahanfar, A.; Vaughan, R.G.; Menon, C. DEA deformed stretchable patch antenna. *Smart Mater. Struct.* **2012**, *21*, 055020. [[CrossRef](#)]
87. Saghlatoon, H.; Honari, M.M.; Mirzavand, R.; Mousavi, P.; Kumar, A.; La, T.G.; Chung, H.J. A novel investigation on printed stretchable WLAN antennas. In Proceedings of the 2017 IEEE International Symposium on Antennas and Propagation & USNC/URSI National Radio Science Meeting, San Diego, CA, USA, 9–14 July 2017; IEEE: Piscataway, NJ, USA, 2017; pp. 2537–2538.
88. Pang, W.; Cheng, X.; Zhao, H.; Guo, X.; Ji, Z.; Li, G.; Liang, Y.; Xue, Z.; Song, H.; Zhang, F.; et al. Electro-mechanically controlled assembly of reconfigurable 3D mesostructures and electronic devices based on dielectric elastomer platforms. *Natl. Sci. Rev.* **2020**, *7*, 342–354. [[CrossRef](#)]
89. Yu, N.; Genevet, P.; Kats, M.A.; Aieta, F.; Tietjen, J.P.; Capasso, F.; Gaburro, Z. Light propagation with phase discontinuities: generalized laws of reflection and refraction. *Science* **2011**, *334*, 333–337. [[CrossRef](#)] [[PubMed](#)]
90. Landgraf, M.; Zorell, U.; Wetzel, T.; Reitelshofer, S.; Yoo, I.S.; Franke, J. Dielectric elastomer actuators as self-sensing devices: A new method of superimposing actuating and sensing signals. In Proceedings of the Electroactive Polymer Actuators and Devices (EAPAD), San Diego, CA, USA, 1 April 2015; Bar-Cohen, Y., Ed.; International Society for Optics and Photonics, SPIE: Bellingham, WA, USA, 2015; Volume 9430, pp. 272–280. [[CrossRef](#)]
91. Huang, P.; Wu, J.; Meng, Q.; Wang, Y.; Su, C.Y. Self-Sensing Motion Control of Dielectric Elastomer Actuator Based on NARX Neural Network and Iterative Learning Control Architecture. In *IEEE/ASME Transactions on Mechatronics*; IEEE: Piscataway, NJ, USA, 2023; pp. 1–11. [[CrossRef](#)]
92. Chortos, A.; Hajjiesmaili, E.; Morales, J.; Clarke, D.R.; Lewis, J.A. 3D Printing of Interdigitated Dielectric Elastomer Actuators. *Adv. Funct. Mater.* **2020**, *30*, 1907375. [[CrossRef](#)]
93. Zou, J.; Gu, G. Dynamic modeling of dielectric elastomer actuators with a minimum energy structure. *Smart Mater. Struct.* **2019**, *28*, 085039. [[CrossRef](#)]
94. Li, W.B.; Zhang, W.M.; Gao, Q.H.; Guo, Q.W.; Wu, S.; Zou, H.X.; Yan, H.; Peng, Z.K.; Meng, G. Electrostatic field induced coupling actuation mechanism for dielectric elastomer actuators. *Extrem. Mech. Lett.* **2020**, *35*, 100638. [[CrossRef](#)]
95. Jia, K.; Lu, T.; Wang, T. Deformation study of an in-plane oscillating dielectric elastomer actuator having complex modes. *J. Sound Vib.* **2019**, *463*, 114940. [[CrossRef](#)]
96. Medina, H.; Farmer, C.W. Improved Model for Conical Dielectric Elastomer Actuators with Fewer Electrical Connections. *J. Mech. Robot.* **2020**, *12*, 031016. [[CrossRef](#)]
97. Farmer, C.; Medina, H. Dimensionless parameter-based numerical model for double conical dielectric elastomer actuators. *Eng. Res. Express* **2020**, *2*, 035020. [[CrossRef](#)]
98. He, T.; Zhao, X.; Suo, Z. Dielectric elastomer membranes undergoing inhomogeneous deformation. *J. Appl. Phys.* **2009**, *106*, 083522. [[CrossRef](#)]

99. Cao, C.; Gao, X.; Burgess, S.; Conn, A.T. Power optimization of a conical dielectric elastomer actuator for resonant robotic systems. *Extrem. Mech. Lett.* **2020**, *35*, 100619. [[CrossRef](#)]
100. Xue, J.; Du, Y.; Zhao, W.; Gao, X. A Modular Crawling Robot Driven by A Single-layer Conical Dielectric Elastomer. In Proceedings of the 2022 IEEE International Conference on Robotics and Biomimetics (ROBIO), Jinghong, China, 5–9 December 2022; IEEE: Piscataway, NJ, USA, 2022; pp. 783–788.
101. Cao, C.; Hill, T.L.; Li, B.; Wang, L.; Gao, X. Nonlinear dynamics of a conical dielectric elastomer oscillator with switchable mono to bi-stability. *Int. J. Solids Struct.* **2021**, *221*, 18–30. [[CrossRef](#)]
102. Zhang, Y.; Wu, J.; Huang, P.; Su, C.Y.; Wang, Y. Inverse dynamics modelling and tracking control of conical dielectric elastomer actuator based on GRU neural network. *Eng. Appl. Artif. Intell.* **2023**, *118*, 105668. [[CrossRef](#)]
103. Mulembo, T.; Njeri, W.; Nagai, G.; Tamagawa, H.; Naito, K.; Nitta, T.; Sasaki, M. Linear-Quadratic Regulator for Control of Multi-Wall Carbon Nanotube/Polydimethylsiloxane Based Conical Dielectric Elastomer Actuators. *Actuators* **2020**, *9*, 18. [[CrossRef](#)]
104. Zou, J.; Gu, G. Feedforward control of the rate-dependent viscoelastic hysteresis nonlinearity in dielectric elastomer actuators. *IEEE Robot. Autom. Lett.* **2019**, *4*, 2340–2347. [[CrossRef](#)]
105. Sun, W.; Liu, F.; Ma, Z.; Li, C.; Zhou, J. Soft mobile robots driven by foldable dielectric elastomer actuators. *J. Appl. Phys.* **2016**, *120*, 084901. [[CrossRef](#)]
106. Timmer, J.; Häußler, S.; Lauk, M.; Lücking, C.H. Pathological tremors: Deterministic chaos or nonlinear stochastic oscillators? *Chaos Interdiscip. J. Nonlinear Sci.* **2000**, *10*, 278–288. [[CrossRef](#)] [[PubMed](#)]
107. Zhang, P.; Yan, Z.; Luo, K.; Tian, Q. Optimal design of electrode topology of dielectric elastomer actuators based on the parameterized level set method. *Soft Robot.* **2023**, *10*, 106–118. [[CrossRef](#)] [[PubMed](#)]
108. Chen, F.; Liu, K.; Wang, Y.; Zou, J.; Gu, G.; Zhu, X. Automatic design of soft dielectric elastomer actuators with optimal spatial electric fields. *IEEE Trans. Robot.* **2019**, *35*, 1150–1165. [[CrossRef](#)]
109. Wang, N.; Guo, H.; Chen, B.; Cui, C.; Zhang, X. Integrated design of actuation and mechanism of dielectric elastomers using topology optimization based on fat Bezier curves. *Soft Robot.* **2019**, *6*, 644–656. [[CrossRef](#)]
110. Zhao, X.; Suo, Z. Method to analyze programmable deformation of dielectric elastomer layers. *Appl. Phys. Lett.* **2008**, *93*, 251902. [[CrossRef](#)]
111. Garnell, E.; Aksoy, B.; Rouby, C.; Shea, H.; Doaré, O. Geometric optimization of dielectric elastomer electrodes for dynamic applications. *Appl. Acoust.* **2021**, *181*, 108120. [[CrossRef](#)]
112. Nalbach, S.; Banda, R.M.; Croce, S.; Rizzello, G.; Naso, D.; Seelecke, S. Modeling and design optimization of a rotational soft robotic system driven by double cone dielectric elastomer actuators. *Front. Robot. AI* **2020**, *6*, 150. [[CrossRef](#)]
113. Arruda, E.M.; Boyce, M.C. A three-dimensional constitutive model for the large stretch behavior of rubber elastic materials. *J. Mech. Phys. Solids* **1993**, *41*, 389–412. [[CrossRef](#)]
114. Edwards, S.; Vilgis, T. The effect of entanglements in rubber elasticity. *Polymer* **1986**, *27*, 483–492. [[CrossRef](#)]
115. Xiang, Y.; Zhong, D.; Wang, P.; Mao, G.; Yu, H.; Qu, S. A general constitutive model of soft elastomers. *J. Mech. Phys. Solids* **2018**, *117*, 110–122. [[CrossRef](#)]
116. Davidson, J.D.; Goulbourne, N.C. A nonaffine network model for elastomers undergoing finite deformations. *J. Mech. Phys. Solids* **2013**, *61*, 1784–1797. [[CrossRef](#)]
117. Rivlin, R. Large elastic deformations of isotropic materials. I. Fundamental concepts. *Philos. Trans. R. Soc. Lond. Ser. A* **1948**, *240*, 459–490.
118. Rivlin, R. Large elastic deformations of isotropic materials IV. Further developments of the general theory. *Philos. Trans. R. Soc. Lond. Ser. A* **1948**, *241*, 379–397.
119. Mooney, M. A theory of large elastic deformation. *J. Appl. Phys.* **1940**, *11*, 582–592. [[CrossRef](#)]
120. Yeoh, O.H. Some forms of the strain energy function for rubber. *Rubber Chem. Technol.* **1993**, *66*, 754–771. [[CrossRef](#)]
121. Ogden, R.W. Large deformation isotropic elasticity—on the correlation of theory and experiment for incompressible rubberlike solids. *Proc. R. Soc. Lond. A* **1972**, *326*, 565–584. [[CrossRef](#)]
122. Treloar, L. Stress-strain data for vulcanized rubber under various types of deformation. *Rubber Chem. Technol.* **1944**, *17*, 813–825. [[CrossRef](#)]
123. Farmer, C.; Medina, H. Hyperelastics.jl: A Julia package for hyperelastic material modelling with a large collection of models. *J. Open Source Softw.* **2024**, *9*, 6314. [[CrossRef](#)]
124. Suo, Z. Theory of dielectric elastomers. *Acta Mech. Solida Sin.* **2010**, *23*, 549–578. [[CrossRef](#)]
125. Di Lillo, L.; Schmidt, A.; Carnelli, D.A.; Ermanni, P.; Kovacs, G.; Mazza, E.; Bergamini, A. Measurement of insulating and dielectric properties of acrylic elastomer membranes at high electric fields. *J. Appl. Phys.* **2012**, *111*, 024904. [[CrossRef](#)]
126. Wissler, M.; Mazza, E. Electromechanical coupling in dielectric elastomer actuators. *Sens. Actuators A Phys.* **2007**, *138*, 384–393. [[CrossRef](#)]
127. Jean-Mistral, C.; Sylvestre, A.; Basrour, S.; Chaillout, J. Dielectric properties of polyacrylate thick films used in sensors and actuators. *Smart Mater. Struct.* **2010**, *19*, 075019. [[CrossRef](#)]
128. Tröls, A.; Kogler, A.; Baumgartner, R.; Kaltseis, R.; Keplinger, C.; Schwödiauer, R.; Graz, I.; Bauer, S. Stretch dependence of the electrical breakdown strength and dielectric constant of dielectric elastomers. *Smart Mater. Struct.* **2013**, *22*, 104012. [[CrossRef](#)]

129. Kuhn, W.; Grün, F. Beziehungen zwischen elastischen Konstanten und Dehnungsdoppelbrechung hochelastischer Stoffe. *Kolloid Z.* **1942**, *101*, 248–271. [[CrossRef](#)]
130. Sheng, J.; Chen, H.; Li, B.; Wang, Y. Influence of the temperature and deformation-dependent dielectric constant on the stability of dielectric elastomers. *J. Appl. Polym. Sci.* **2013**, *128*, 2402–2407. [[CrossRef](#)]
131. Brokate, M.; Sprekels, J. *Hysteresis and Phase Transitions*; Springer Science & Business Media: Berlin/Heidelberg, Germany, 2012; Volume 121.
132. Khurana, A.; Kumar, A.; Raut, S.K.; Sharma, A.K.; Joglekar, M.M. Effect of viscoelasticity on the nonlinear dynamic behavior of dielectric elastomer minimum energy structures. *Int. J. Solids Struct.* **2021**, *208*, 141–153. [[CrossRef](#)]
133. Alibakhshi, A.; Heidari, H. Nonlinear dynamics of dielectric elastomer balloons based on the Gent-Gent hyperelastic model. *Eur. J. Mech. A/Solids* **2020**, *82*, 103986. [[CrossRef](#)]
134. Chen, Y.; Kang, G.; Yuan, J.; Hu, Y.; Li, T.; Qu, S. An electro-mechanically coupled visco-hyperelastic-plastic constitutive model for cyclic deformation of dielectric elastomers. *Mech. Mater.* **2020**, *150*, 103575. [[CrossRef](#)]
135. Alibakhshi, A.; Chen, W.; Destrade, M. Nonlinear vibration and stability of a dielectric elastomer balloon based on a strain-stiffening model. *J. Elast.* **2023**, *153*, 533–548. [[CrossRef](#)]
136. Chiang Foo, C.; Cai, S.; Jin Adrian Koh, S.; Bauer, S.; Suo, Z. Model of dissipative dielectric elastomers. *J. Appl. Phys.* **2012**, *111*, 034102. [[CrossRef](#)]
137. Zhao, X.; Hong, W.; Suo, Z. Electromechanical hysteresis and coexistent states in dielectric elastomers. *Phys. Rev. B* **2007**, *76*, 134113. [[CrossRef](#)]
138. Amin, A.; Lion, A.; Sekita, S.; Okui, Y. Nonlinear dependence of viscosity in modeling the rate-dependent response of natural and high damping rubbers in compression and shear: Experimental identification and numerical verification. *Int. J. Plast.* **2006**, *22*, 1610–1657. [[CrossRef](#)]
139. Rey, T.; Chagnon, G.; Le Cam, J.B.; Favier, D. Influence of the temperature on the mechanical behaviour of filled and unfilled silicone rubbers. *Polym. Test.* **2013**, *32*, 492–501. [[CrossRef](#)]
140. Bergström, J.S.; Boyce, M.C. Constitutive modeling of the large strain time-dependent behavior of elastomers. *J. Mech. Phys. Solids* **1998**, *46*, 931–954. [[CrossRef](#)]
141. Lion, A. On the large deformation behaviour of reinforced rubber at different temperatures. *J. Mech. Phys. Solids* **1997**, *45*, 1805–1834. [[CrossRef](#)]
142. Lion, A. Constitutive modelling in finite thermoviscoplasticity: A physical approach based on nonlinear rheological models. *Int. J. Plast.* **2000**, *16*, 469–494. [[CrossRef](#)]
143. Lion, A. Thixotropic behaviour of rubber under dynamic loading histories: Experiments and theory. *J. Mech. Phys. Solids* **1998**, *46*, 895–930. [[CrossRef](#)]
144. Miehe, C.; Keck, J. Superimposed finite elastic–viscoelastic–plastoelastic stress response with damage in filled rubbery polymers. Experiments, modelling and algorithmic implementation. *J. Mech. Phys. Solids* **2000**, *48*, 323–365. [[CrossRef](#)]
145. Guélin, P. Remarques sur L’hysteresis Mecanique. Les Bases d’un Schema Thermomecanique a Structure Hereditaire. *J. Mec.* **1980**, *19*, 217–247.
146. Krempl, E.; Khan, F. Rate (time)-dependent deformation behavior: An overview of some properties of metals and solid polymers. *Int. J. Plast.* **2003**, *19*, 1069–1095. [[CrossRef](#)]
147. Laiarinandrasana, L.; Piques, R.; Robisson, A. Visco-hyperelastic model with internal state variable coupled with discontinuous damage concept under total Lagrangian formulation. *Int. J. Plast.* **2003**, *19*, 977–1000. [[CrossRef](#)]
148. Haupt, P.; Sedlan, K. Viscoplasticity of elastomeric materials: Experimental facts and constitutive modelling. *Arch. Appl. Mech.* **2001**, *71*, 89–109. [[CrossRef](#)]
149. Hasanpour, K.; Ziaei-Rad, S.; Mahzoon, M. A large deformation framework for compressible viscoelastic materials: Constitutive equations and finite element implementation. *Int. J. Plast.* **2009**, *25*, 1154–1176. [[CrossRef](#)]
150. Kilian, H.; Strauss, M.; Hamm, W. Universal properties in filler-loaded rubbers. *Rubber Chem. Technol.* **1994**, *67*, 1–16. [[CrossRef](#)]
151. Mathew, A.T.; Vo, T.V.K.; Koh, S.J.A. A molecular perspective to analytical modeling that reveals new instabilities in dielectric elastomer transducers. *J. Mech. Phys. Solids* **2019**, *132*, 103703. [[CrossRef](#)]
152. Li, B.; Chen, H.; Qiang, J.; Hu, S.; Zhu, Z.; Wang, Y. Effect of mechanical pre-stretch on the stabilization of dielectric elastomer actuation. *J. Phys. D Appl. Phys.* **2011**, *44*, 155301. [[CrossRef](#)]
153. Plante, J.S.; Dubowsky, S. Large-scale failure modes of dielectric elastomer actuators. *Int. J. Solids Struct.* **2006**, *43*, 7727–7751. [[CrossRef](#)]
154. Godaba, H.; Zhang, Z.Q.; Gupta, U.; Foo, C.C.; Zhu, J. Instabilities in dielectric elastomers: Buckling, wrinkling, and crumpling. *Soft Matter* **2019**, *15*, 7137–7144. [[CrossRef](#)]
155. Zhu, J.; Kolloosche, M.; Lu, T.; Kofod, G.; Suo, Z. Two types of transitions to wrinkles in dielectric elastomers. *Soft Matter* **2012**, *8*, 8840–8846. [[CrossRef](#)]
156. Mao, G.; Wu, L.; Liang, X.; Qu, S. Morphology of voltage-triggered ordered wrinkles of a dielectric elastomer sheet. *J. Appl. Mech.* **2017**, *84*, 111005. [[CrossRef](#)]
157. Zurlo, G.; Destrade, M.; DeTommasi, D.; Puglisi, G. Catastrophic thinning of dielectric elastomers. *Phys. Rev. Lett.* **2017**, *118*, 078001. [[CrossRef](#)]

158. Sheima, Y.; Caspari, P.; Opris, D.M. Artificial muscles: Dielectric elastomers responsive to low voltages. *Macromol. Rapid Commun.* **2019**, *40*, 1900205. [[CrossRef](#)]
159. Kumar, D.; Sarangi, S. Pre-stretch and frequency variation effect on the dielectric permittivity of a dielectric elastomer: An amended permittivity model. *Sādhanā* **2019**, *44*, 173. [[CrossRef](#)]
160. Pelrine, R.; Kornbluh, R.; Pei, Q.; Joseph, J. High-speed electrically actuated elastomers with strain greater than 100%. *Science* **2000**, *287*, 836–839. [[CrossRef](#)] [[PubMed](#)]
161. Zhao, X.; Suo, Z. Theory of dielectric elastomers capable of giant deformation of actuation. *Phys. Rev. Lett.* **2010**, *104*, 178302. [[CrossRef](#)]
162. Liu, L.; Liu, Y.; Li, B.; Yang, K.; Li, T.; Leng, J. Thermo-electro-mechanical instability of dielectric elastomers. *Smart Mater. Struct.* **2011**, *20*, 075004. [[CrossRef](#)]
163. Huang, J.; Shian, S.; Diebold, R.M.; Suo, Z.; Clarke, D.R. The thickness and stretch dependence of the electrical breakdown strength of an acrylic dielectric elastomer. *Appl. Phys. Lett.* **2012**, *101*, 122905. [[CrossRef](#)]
164. Kofod, G.; Sommer-Larsen, P.; Kornbluh, R.; Pelrine, R. Actuation response of polyacrylate dielectric elastomers. *J. Intell. Mater. Syst. Struct.* **2003**, *14*, 787–793. [[CrossRef](#)]
165. Zhao, Y.; Zha, J.W.; Yin, L.J.; Gao, Z.S.; Wen, Y.Q.; Dang, Z.M. Remarkable electrically actuation performance in advanced acrylic-based dielectric elastomers without pre-strain at very low driving electric field. *Polymer* **2018**, *137*, 269–275. [[CrossRef](#)]
166. Kofod, G. The static actuation of dielectric elastomer actuators: How does pre-stretch improve actuation? *J. Phys. D Appl. Phys.* **2008**, *41*, 215405. [[CrossRef](#)]
167. Khanh, V.T.V.; Mathew, A.T.; Short, J.S.; Quek, Z.F.; Ang, M.H.; Koh, S.J.A. Displacement improvement from variable pre-stretch diaphragm type Dielectric Elastomer Actuator. In Proceedings of the 2018 IEEE/ASME International Conference on Advanced Intelligent Mechatronics (AIM), Auckland, New Zealand, 9–12 July 2018; IEEE: Piscataway, NJ, USA, 2018; pp. 545–550.
168. Pelrine, R.; Sommer-Larsen, P.; Kornbluh, R.D.; Heydt, R.; Kofod, G.; Pei, Q.; Gravesen, P. Applications of dielectric elastomer actuators. In Proceedings of the Smart Structures and Materials 2001: Electroactive Polymer Actuators and Devices, San Diego, CA, USA, 17–21 March 2001; International Society for Optics and Photonics: Bellingham, WA, USA, 2001; Volume 4329, pp. 335–349.
169. Dughaiash, Z.H. Dielectric properties of $(\text{BaTiO}_3)_{1-x}(\text{SnO}_2)_x$ ceramics. *J. Nat. Sci. Math.* **2013**, *6*, 107–121. [[CrossRef](#)]
170. Zou, J.; Gu, G.Y.; Zhu, L.M. Open-loop control of creep and vibration in dielectric elastomer actuators with phenomenological models. *IEEE/ASME Trans. Mechatron.* **2016**, *22*, 51–58. [[CrossRef](#)]
171. McKay, T.; O'Brien, B.; Calius, E.; Anderson, I. An integrated, self-priming dielectric elastomer generator. *Appl. Phys. Lett.* **2010**, *97*, 062911. [[CrossRef](#)]
172. Zhang, J.; Tang, L.; Liu, L.; Zhao, J.; Yang, Z.; Li, P. Modeling of humidity effect on electromechanical properties of viscoelastic dielectric elastomer. *Int. J. Mech. Sci.* **2021**, *193*, 106177. [[CrossRef](#)]
173. Zuo, Y.; Ding, Y.; Zhang, J.; Zhu, M.; Liu, L.; Zhao, J. Humidity effect on dynamic electromechanical properties of polyacrylic dielectric elastomer: An experimental study. *Polymers* **2021**, *13*, 784. [[CrossRef](#)]
174. Liu, X.; Zhang, J.; Chen, H. Ambient humidity altering electromechanical actuation of dielectric elastomers. *Appl. Phys. Lett.* **2019**, *115*, 184101. [[CrossRef](#)]
175. Albuquerque, F.B.; Shea, H. Influence of humidity, temperature and prestretch on the dielectric breakdown strength of silicone elastomer membranes for DEAs. *Smart Mater. Struct.* **2020**, *29*, 105024. [[CrossRef](#)]
176. Plante, J.S.; Dubowsky, S. On the properties of dielectric elastomer actuators and their design implications. *Smart Mater. Struct.* **2007**, *16*, S227. [[CrossRef](#)]
177. Mathew, A.T.; Koh, S.J.A. Operational limits of a non-homogeneous dielectric elastomer transducer. *Int. J. Smart Nano Mater.* **2017**, *8*, 214–231. [[CrossRef](#)]
178. Seifi, S.; Park, H.S. Electro-elastocapillary Rayleigh–plateau instability in dielectric elastomer films. *Soft Matter* **2017**, *13*, 4305–4310. [[CrossRef](#)]
179. Romasanta, L.J.; Lopez-Manchado, M.Á.; Verdejo, R. Increasing the performance of dielectric elastomer actuators: A review from the materials perspective. *Prog. Polym. Sci.* **2015**, *51*, 188–211. [[CrossRef](#)]
180. Ha, S.M.; Yuan, W.; Pei, Q.; Pelrine, R.; Stanford, S. Interpenetrating polymer networks for high-performance electroelastomer artificial muscles. *Adv. Mater.* **2006**, *18*, 887–891. [[CrossRef](#)]
181. Ha, S.M.; Yuan, W.; Pei, Q.; Pelrine, R.; Stanford, S. Interpenetrating networks of elastomers exhibiting 300% electrically-induced area strain. *Smart Mater. Struct.* **2007**, *16*, S280. [[CrossRef](#)]
182. Sahu, D.; Sahu, R.K.; Patra, K. Effects of crosslink density on the behavior of VHB 4910 dielectric elastomer. *J. Macromol. Sci. Part A* **2019**, *56*, 821–829. [[CrossRef](#)]
183. Tugui, C.; Bele, A.; Tiron, V.; Hamciuc, E.; Varganici, C.D.; Cazacu, M. Dielectric elastomers with dual piezo-electrostatic response optimized through chemical design for electromechanical transducers. *J. Mater. Chem. C* **2017**, *5*, 824–834. [[CrossRef](#)]
184. Xu, J.; Dong, Y.; Jiang, Z.; Tang, L.; Chen, X.; Yao, Z.; Cao, K. Self-healing high-performance dielectric elastomer actuator with novel liquid-solid interpenetrating structure. *Compos. Part A Appl. Sci. Manuf.* **2021**, *149*, 106519. [[CrossRef](#)]
185. Utrera-Barrios, S.; Verdejo, R.; López-Manchado, M.A.; Santana, M.H. Evolution of self-healing elastomers, from extrinsic to combined intrinsic mechanisms: A review. *Mater. Horiz.* **2020**, *7*, 2882–2902. [[CrossRef](#)]
186. Bilodeau, R.A.; Kramer, R.K. Self-healing and damage resilience for soft robotics: A review. *Front. Robot. AI* **2017**, *4*, 48. [[CrossRef](#)]

187. Bortot, E.; Springhetti, R.; Gei, M. Enhanced soft dielectric composite generators: The role of ceramic fillers. *J. Eur. Ceram. Soc.* **2014**, *34*, 2623–2632. [[CrossRef](#)]
188. Gallone, G.; Galantini, F.; Carpi, F. Perspectives for new dielectric elastomers with improved electromechanical actuation performance: Composites versus blends. *Polym. Int.* **2010**, *59*, 400–406. [[CrossRef](#)]
189. Zhang, Z.; Liu, L.; Fan, J.; Yu, K.; Liu, Y.; Shi, L.; Leng, J. New silicone dielectric elastomers with a high dielectric constant. In Proceedings of the Modeling, Signal Processing, and Control for Smart Structures, San Diego, CA, USA, 9–13 March 2008; International Society for Optics and Photonics: Bellingham, WA, USA, 2008; Volume 6926, p. 692610.
190. Gallone, G.; Carpi, F.; De Rossi, D.; Levita, G.; Marchetti, A. Dielectric constant enhancement in a silicone elastomer filled with lead magnesium niobate–lead titanate. *Mater. Sci. Eng. C* **2007**, *27*, 110–116. [[CrossRef](#)]
191. Carpi, F.; Rossi, D.D. Improvement of electromechanical actuating performances of a silicone dielectric elastomer by dispersion of titanium dioxide powder. *IEEE Trans. Dielectr. Electr. Insul.* **2005**, *12*, 835–843. [[CrossRef](#)]
192. Ruan, M.; Yang, D.; Guo, W.; Zhang, L.; Wu, Y.; Li, S. Mussel-inspired synthesis of barium titanate@ poly (dopamine)@ graphene oxide multilayer core-shell hybrids for high-performance dielectric elastomer actuator. *Mater. Lett.* **2018**, *219*, 109–113. [[CrossRef](#)]
193. Ning, N.; Ma, Q.; Liu, S.; Tian, M.; Zhang, L.; Nishi, T. Tailoring dielectric and actuated properties of elastomer composites by bioinspired poly (dopamine) encapsulated graphene oxide. *ACS Appl. Mater. Interfaces* **2015**, *7*, 10755–10762. [[CrossRef](#)]
194. Banet, P.; Zeggai, N.; Chavanne, J.; Nguyen, G.T.; Chikh, L.; Plesse, C.; Almanza, M.; Martinez, T.; Civet, Y.; Perriard, Y.; et al. Evaluation of dielectric elastomers to develop materials suitable for actuation. *Soft Matter* **2021**, *17*, 10786–10805. [[CrossRef](#)]
195. Skov, A.L.; Yu, L. Optimization Techniques for Improving the Performance of Silicone-Based Dielectric Elastomers. *Adv. Eng. Mater.* **2018**, *20*, 1700762. [[CrossRef](#)]
196. Tan, M.W.M.; Thangavel, G.; Lee, P.S. Enhancing dynamic actuation performance of dielectric elastomer actuators by tuning viscoelastic effects with polar crosslinking. *NPG Asia Mater.* **2019**, *11*, 62. [[CrossRef](#)]
197. Yu, L.; Madsen, F.B.; Hvilsted, S.; Skov, A.L. High energy density interpenetrating networks from ionic networks and silicone. In Proceedings of the Electroactive Polymer Actuators and Devices (EAPAD), San Diego, CA, USA, 8–12 March 2015; SPIE: Bellingham, WA, USA, 2015; Volume 9430, pp. 196–206.
198. Zhang, Y.; Ellingford, C.; Zhang, R.; Roscow, J.; Hopkins, M.; Keogh, P.; McNally, T.; Bowen, C.; Wan, C. Electrical and mechanical self-healing in high-performance dielectric elastomer actuator materials. *Adv. Funct. Mater.* **2019**, *29*, 1808431. [[CrossRef](#)]
199. Fan, F.; Szpunar, J. Characterization of viscoelasticity and self-healing ability of VHB 4910. *Macromol. Mater. Eng.* **2015**, *300*, 99–106. [[CrossRef](#)]
200. Chen, Y.; Agostini, L.; Moretti, G.; Fontana, M.; Vertechy, R. Dielectric elastomer materials for large-strain actuation and energy harvesting: A comparison between styrenic rubber, natural rubber and acrylic elastomer. *Smart Mater. Struct.* **2019**, *28*, 114001. [[CrossRef](#)]
201. Madsen, F.B.; Daugaard, A.E.; Hvilsted, S.; Skov, A.L. The current state of silicone-based dielectric elastomer transducers. *Macromol. Rapid Commun.* **2016**, *37*, 378–413. [[CrossRef](#)]
202. Cameron, C.G.; Underhill, R.S.; Rawji, M.; Szabo, J.P. Conductive filler: Elastomer composites for Maxwell stress actuator applications. In Proceedings of the Smart Structures and Materials 2004: Electroactive Polymer Actuators and Devices (EAPAD), San Diego, CA, USA, 14–18 March 2004; International Society for Optics and Photonics: Bellingham, WA, USA, 2004; Volume 5385, pp. 51–59.
203. Zhang, Q.P.; Liu, J.H.; Liu, H.D.; Jia, F.; Zhou, Y.L.; Zheng, J. Tailoring chain length and cross-link density in dielectric elastomer toward enhanced actuation strain. *Appl. Phys. Lett.* **2017**, *111*, 152901. [[CrossRef](#)]
204. Yang, D.; Tian, M.; Kang, H.; Dong, Y.; Liu, H.; Yu, Y.; Zhang, L. New polyester dielectric elastomer with large actuated strain at low electric field. *Mater. Lett.* **2012**, *76*, 229–232. [[CrossRef](#)]
205. Sun, H.; Liu, X.; Yan, H.; Feng, Z.; Yu, B.; Ning, N.; Tian, M.; Zhang, L. The role of dipole structure and their interaction on the electromechanical and actuation performance of homogeneous silicone dielectric elastomers. *Polymer* **2019**, *165*, 1–10. [[CrossRef](#)]
206. Su, Y.; Sui, G.; Lan, J.; Yang, X. A highly stretchable dielectric elastomer based on core–shell structured soft polymer-coated liquid-metal nanofillers. *Chem. Commun.* **2020**, *56*, 11625–11628. [[CrossRef](#)]
207. Ziegmann, A.; Schubert, D.W. Influence of the particle size and the filling degree of barium titanate filled silicone elastomers used as potential dielectric elastomers on the mechanical properties and the crosslinking density. *Mater. Today Commun.* **2018**, *14*, 90–98. [[CrossRef](#)]
208. Chen, T.; Lin, M.; Zhao, Y.; Pan, L.; Tang, Q. Electromechanical response of polyol-polyurethane blends as dielectric elastomer flexible micro-actuator material. *J. Mater. Sci. Mater. Electron.* **2017**, *28*, 3560–3570. [[CrossRef](#)]
209. Ning, N.; Qin, H.; Wang, M.; Sun, H.; Tian, M.; Zhang, L. Improved dielectric and actuated performance of thermoplastic polyurethane by blending with XNBR as macromolecular dielectrics. *Polymer* **2019**, *179*, 121646. [[CrossRef](#)]
210. Ye, Z.; Chen, Z.; Asmatulu, R.; Chan, H. Robust control of dielectric elastomer diaphragm actuator for human pulse signal tracking. *Smart Mater. Struct.* **2017**, *26*, 085043. [[CrossRef](#)]
211. Massenio, P.R.; Rizzello, G.; Comitangelo, G.; Naso, D.; Seelecke, S. Reinforcement Learning-Based Minimum Energy Position Control of Dielectric Elastomer Actuators. *IEEE Trans. Control Syst. Technol.* **2020**, *29*, 1674–1688. [[CrossRef](#)]
212. Li, L.; Li, J.; Qin, L.; Cao, J.; Kankanhalli, M.S.; Zhu, J. Deep Reinforcement Learning in Soft Viscoelastic Actuator of Dielectric Elastomer. *IEEE Robot. Autom. Lett.* **2019**, *4*, 2094–2100. [[CrossRef](#)]

213. Huang, P.; Wu, J.; Zhang, P.; Wang, Y.; Su, C.Y. Dynamic modeling and tracking control for dielectric elastomer actuator with a model predictive controller. *IEEE Trans. Ind. Electron.* **2021**, *69*, 1819–1828. [CrossRef]
214. Tao, B.; Luo, K.; Tian, Q.; Hu, H. Inverse dynamic design for motion control of soft machines driven by dielectric elastomer actuators. *Int. J. Mech. Sci.* **2024**, *273*, 109213. [CrossRef]
215. Branz, F.; Francesconi, A. Modelling and control of double-cone dielectric elastomer actuator. *Smart Mater. Struct.* **2016**, *25*, 095040. [CrossRef]
216. Braganza, D.; Dawson, D.M.; Walker, I.D.; Nath, N. A Neural Network Controller for Continuum Robots. *IEEE Trans. Robot.* **2007**, *23*, 1270–1277. [CrossRef]
217. Xian, B.; Dawson, D.; de Queiroz, M.; Chen, J. A Continuous Asymptotic Tracking Control Strategy for Uncertain Nonlinear Systems. *IEEE Trans. Autom. Control* **2004**, *49*, 1206–1211. [CrossRef]
218. Chin, K.; Hellebrekers, T.; Majidi, C. Machine Learning for Soft Robotic Sensing and Control. *Adv. Intell. Syst.* **2020**, *2*, 1900171. [CrossRef]
219. Abbeel, P.; Quigley, M.; Ng, A.Y. Using Inaccurate Models in Reinforcement Learning. In Proceedings of the 23rd International Conference on Machine Learning—ICML '06, Pittsburgh, PA, USA, 25–29 June 2006; ACM Press: Pittsburgh, PA, USA, 2006; pp. 1–8. [CrossRef]
220. Medina, H.; Gentry, N.; Farmer, C. Remote Laboratory for Machine Learning Training of a Soft Actuator's Control: A Case Study. In Proceedings of the 2021 ASEE Southeastern Section Conference, Virtual, 7–10 March 2021.
221. Francois-Lavet, V.; Henderson, P.; Islam, R.; Bellemare, M.G.; Pineau, J. An Introduction to Deep Reinforcement Learning. *Found. Trends Mach. Learn.* **2018**, *11*, 219–354. [CrossRef]
222. Kirkpatrick, K.; Valasek, J.; Haag, C. Characterization and Control of Hysteretic Dynamics Using Online Reinforcement Learning. *J. Aerosp. Inf. Syst.* **2013**, *10*, 297–305. [CrossRef]
223. Osman, H.E. On Reinforcement Memory for Non-Markovian Control. In *Research and Development in Intelligent Systems XXVII*; Bramer, M., Petridis, M., Hopgood, A., Eds.; Springer: London, UK, 2011; pp. 179–192. [CrossRef]
224. Hausknecht, M.; Stone, P. Deep recurrent q-learning for partially observable mdps. In Proceedings of the 2015 AAAI Fall Symposium Series, Arlington, Virginia, 12–14 November 2015.
225. Liu, V.; Adeniji, A.; Lee, N.; Zhao, J.; Srouji, M. Recurrent Control Nets for Deep Reinforcement Learning. *arXiv* **2019**, arXiv:1901.01994. <https://doi.org/10.48550/arXiv.1901.01994>.
226. Chen, C.; Ying, V.; Laird, D. Deep Q-Learning with Recurrent Neural Networks. *Stanf. Cs229 Course Rep.* **2016**, *4*, 6.
227. Kalashnikov, D.; Irpan, A.; Pastor, P.; Ibarz, J.; Herzog, A.; Jang, E.; Quillen, D.; Holly, E.; Kalakrishnan, M.; Vanhoucke, V.; et al. Scalable Deep Reinforcement Learning for Vision-Based Robotic Manipulation In Proceedings of the 2nd Conference on Robot Learning, Zurich, Switzerland, 29–31 October 2018; Billard, A., Dragan, A., Peters, J., Morimoto, J., Eds.; Proceedings of Machine Learning Research; PMLR; 2018; Volume 87, pp. 651–673.
228. Rueckert, E.; Nakatenus, M.; Tosatto, S.; Peters, J. Learning Inverse Dynamics Models in $O(n)$ Time with LSTM Networks. In Proceedings of the 2017 IEEE-RAS 17th International Conference on Humanoid Robotics (Humanoids), Birmingham, UK, 15–17 November 2017; IEEE: Birmingham, UK, 2017; pp. 811–816. [CrossRef]
229. Thuruthel, T.G.; Shih, B.; Laschi, C.; Tolley, M.T. Soft Robot Perception Using Embedded Soft Sensors and Recurrent Neural Networks. *Sci. Robot.* **2019**, *4*, eaav1488. [CrossRef]
230. Veeramani, A.S.; Crews, J.H.; Buckner, G.D. Hysteretic Recurrent Neural Networks: A Tool for Modeling Hysteretic Materials and Systems. *Smart Mater. Struct.* **2009**, *18*, 075004. [CrossRef]
231. Gonzalez, J.; Yu, W. Non-Linear System Modeling Using LSTM Neural Networks. *IFAC-Pap.* **2018**, *51*, 485–489. [CrossRef]
232. Omidshafiei, S.; Pazis, J.; Amato, C.; How, J.P.; Vian, J. Deep Decentralized Multi-task Multi-Agent Reinforcement Learning under Partial Observability. In Proceedings of the 34th International Conference on Machine Learning, Sydney, NSW, Australia, 6–11 August 2017; Precup, D., Teh, Y.W., Eds.; Proceedings of Machine Learning Research; PMLR; 2017; Volume 70, pp. 2681–2690.
233. Yang, T.; Xiao, Y.; Zhang, Z.; Liang, Y.; Li, G.; Zhang, M.; Li, S.; Wong, T.W.; Wang, Y.; Li, T.; et al. A Soft Artificial Muscle Driven Robot With Reinforcement Learning. *Sci. Rep.* **2018**, *8*, 14518. [CrossRef]
234. Larson, C.; Spjut, J.; Knepper, R.; Shepherd, R. A Deformable Interface for Human Touch Recognition Using Stretchable Carbon Nanotube Dielectric Elastomer Sensors and Deep Neural Networks. *Soft Robot.* **2019**, *6*, 611–620. [CrossRef] [PubMed]
235. Raissi, M.; Perdikaris, P.; Karniadakis, G.E. Physics-Informed Neural Networks: A Deep Learning Framework for Solving Forward and Inverse Problems Involving Nonlinear Partial Differential Equations. *J. Comput. Phys.* **2019**, *378*, 686–707. [CrossRef]
236. Gaskett, C.; Wettergreen, D.; Zelinsky, A. Q-learning in continuous state and action spaces. In Proceedings of the Australasian Joint Conference on Artificial Intelligence, Sydney, Australia, 6–10 December 1999; Springer: Berlin/Heidelberg, Germany, 1999; pp. 417–428.
237. Baydere, B.A.; Talas, S.K.; Samur, E. A novel highly-extensible 2-DOF pneumatic actuator for soft robotic applications. *Sens. Actuators A Phys.* **2018**, *281*, 84–94. [CrossRef]
238. Rizzello, G.; Naso, D.; York, A.; Seelecke, S. A self-sensing approach for dielectric elastomer actuators based on online estimation algorithms. *IEEE/ASME Trans. Mechatron.* **2016**, *22*, 728–738. [CrossRef]
239. Sánchez-Solano, S.; Cabrera, A.J.; Baturone, I.; Moreno-Velo, F.J.; Brox, M. FPGA implementation of embedded fuzzy controllers for robotic applications. *IEEE Trans. Ind. Electron.* **2007**, *54*, 1937–1945. [CrossRef]

240. Wang, Y.; Xu, J.; Han, Y.; Li, H.; Li, X. DeepBurning: Automatic generation of FPGA-based learning accelerators for the neural network family. In Proceedings of the 2016 53rd ACM/EDAC/IEEE Design Automation Conference (DAC), Austin, TX, USA, 5–9 June 2016; IEEE: Piscataway, NJ, USA, 2016; pp. 1–6.
241. Su, J.; Liu, J.; Thomas, D.B.; Cheung, P.Y. Neural network based reinforcement learning acceleration on FPGA platforms. *ACM SIGARCH Comput. Archit. News* **2017**, *44*, 68–73. [[CrossRef](#)]
242. Zhang, C.; Li, P.; Sun, G.; Guan, Y.; Xiao, B.; Cong, J. Optimizing fpga-based accelerator design for deep convolutional neural networks. In Proceedings of the 2015 ACM/SIGDA International Symposium on Field-Programmable Gate Arrays, Monterey, CA, USA, 22–24 February 2015; pp. 161–170.
243. Da Silva, L.M.; Torquato, M.F.; Fernandes, M.A. Parallel implementation of reinforcement learning q-learning technique for fpga. *IEEE Access* **2018**, *7*, 2782–2798. [[CrossRef](#)]
244. Leong, P.H.W.; Tsoi, K.H. Field Programmable Gate Array technology for robotics applications. In Proceedings of the 2005 IEEE International Conference on Robotics and Biomimetics-ROBIO, Shatin, China, 5–9 July 2005; IEEE: Piscataway, NJ, USA, 2005; pp. 295–298.
245. Arish, S.; Sharma, R. Run-Time-Reconfigurable Multi-Precision Floating-Point Matrix Multiplier Intellectual Property Core on FPGA. *Circuits Syst. Signal Process.* **2017**, *36*, 998–1026. [[CrossRef](#)]
246. Wei, H.; Li, C.; Chen, D.; Wang, J.; Wang, T. Research on reconfigurable robot controller based on ARM and FPGA. In Proceedings of the 2008 6th IEEE International Conference on Industrial Informatics, Daejeon, Republic of Korea, 13–16 July 2008; IEEE: Piscataway, NJ, USA, 2008; pp. 123–128.
247. Astarloa, A.; Lázaro, J.; Bidarte, U.; Jiménez, J.; Zuloaga, A. FPGA technology for multi-axis control systems. *Mechatronics* **2009**, *19*, 258–268. [[CrossRef](#)]
248. Upegui, A.; Moeckel, R.; Dittrich, E.; Ijspeert, A.; Sanchez, E. An FPGA dynamically reconfigurable framework for modular robotics. In Proceedings of the Workshop Proceedings of the 18th International Conference on Architecture of Computing Systems 2005 (ARCS'05), Innsbruck, Austria, 14–17 March 2005; VDE Verlag: Berlin, Germany, 2005; number CONF.
249. Hill, M.; Rizzello, G.; Seelecke, S. Development of a fatigue testing setup for dielectric elastomer membrane actuators. In Proceedings of the Electroactive Polymer Actuators and Devices (EAPAD), Portland, OR, USA, 26–29 March 2017; International Society for Optics and Photonics: Bellingham, WA, USA, 2017; Volume 10163, p. 101630X.
250. Atalik, T.; Deniz, M.; Koc, E.; Gercek, C.O.; Gultekin, B.; Ermis, M.; Cadirci, I. Multi-DSP and -FPGA-Based Fully Digital Control System for Cascaded Multilevel Converters Used in FACTS Applications. *IEEE Trans. Ind. Inform.* **2012**, *8*, 511–527. [[CrossRef](#)]
251. Bonato, V.; Peron, R.; Wolf, D.F.; de Holanda, J.A.; Marques, E.; Cardoso, J.M. An FPGA implementation for a Kalman filter with application to mobile robotics. In Proceedings of the 2007 International Symposium on Industrial Embedded Systems, Lisbon, Portugal, 4–6 July 2007; IEEE: Piscataway, NJ, USA, 2007; pp. 148–155.
252. Van Duong, L.; Asahina, R.; Wang, J. Development of a vision-based soft tactile muscularis. In Proceedings of the 2019 2nd IEEE International Conference on Soft Robotics (RoboSoft), Seoul, Republic of Korea, 14–18 April 2019; IEEE: Piscataway, NJ, USA, 2019; pp. 343–348.
253. Gankidi, P.R. Fpga Accelerator Architecture for Q-Learning and Its Applications in Space Exploration Rovers. Ph.D. Thesis, Arizona State University, Tempe, AZ, USA, 2016.
254. Deiss, S.R.; Douglas, R.J.; Whatley, A.M.; Maass, W. A pulse-coded communications infrastructure for neuromorphic systems. *Pulsed Neural Netw.* **1999**, 157–178. [[CrossRef](#)]
255. Upegui, A.; Pena-Reyes, C.A.; Sanchez, E. An FPGA platform for on-line topology exploration of spiking neural networks. *Microprocess. Microsyst.* **2005**, *29*, 211–223. [[CrossRef](#)]

Disclaimer/Publisher's Note: The statements, opinions and data contained in all publications are solely those of the individual author(s) and contributor(s) and not of MDPI and/or the editor(s). MDPI and/or the editor(s) disclaim responsibility for any injury to people or property resulting from any ideas, methods, instructions or products referred to in the content.